Study of Structural and Optical Properties of Undoped and Rare Earth Doped TiO_2 Nanostructures

By

Tsholo Ernest Talane

Submitted in accordance with the requirements
for the degree of

MASTER OF SCIENCE

In the subject

PHYSICS

at the

UNIVERSITY OF SOUTH

AFRICA

SUPERVISOR: PROF. M S DHLAMINI

CO-SUPERVISORS: PROF. B M MOTHUDI

: DR G H MHLONGO

2017

Declaration

(Student number: 5333-361-6)

I declare that "STUDY OF STRUCTURAL AND OPTICAL PROPERTIES OF UNDOPED AND RARE EARTH DOPED TiO_2" is my own work and that all sources that I have used or quoted have been indicated and acknowledged by means of complete references.

_____ _____

SIGNATURE DATE

(Tsholo Ernest Talane)

Acknowledgements

- First and foremost I would like to say thanks to God Almighty for his guidance and protection throughout my study.
- To my thesis advisor, Prof. M.S Dhlamini for his continuous support of my MSc study and research, for his motivation and immense knowledge.
- My sincere gratitude to Dr. G.H Mhlongo, Dr. LL Noto, and Prof. BK Mothudi as the second readers of this thesis, I am gratefully indebted to their very valuable comments.
- I would also like to acknowledge the help of my lab partners, Dr. G.L Kabongo, Mr. S Mofokeng, Mr. FV Molefe, Mrs. L Mathevula, Mr. C Manaka, and Dr. P Mbule for their passionate participation and input.
- Great thanks to the funders of this research project, National Research Foundation (NRF), Grow Your Own Timber (GYOT) and University of South Africa (UNISA). The Department of Physics has provided the support and equipment I have needed to produce and complete my thesis.
- Finally, I must express my very profound gratitude to my mother Mrs. LM Talane, my life partner Ms. M.A Mofokeng for their unfailing support and continuous encouragement throughout my years of study and a special dedication to my lovely daughter, Rethabile Talane for enduring long periods of time without me by her side.

Thesis dedicated to the memory of the late Mrs. Maki Miya (1962-2017), O robale ka kgotso Mosia.

A special dedication to my late father Mr. Maswetsa Talane (1941-2018), a strong and a smart gentleman whom I still miss every day (robala ka kgotso Motaung)

Summary

Un-doped, Er^{3+} doped (TiO_2:Er^{3+}) as well as Er^{3+}/Yb^{3+} co-doped (TiO_2:Er^{3+}/Yb^{3+}) nanocrystals with different concentrations of RE^{3+} (Er^{3+}, Yb^{3+}) were successfully synthesized using the sol-gel method.

The powder X-ray diffraction (XRD) spectra revealed that all undoped and doped samples remained in anatase after annealing at 400°C. The presence of RE^{3+} ions in the TiO_2 host lattice was confirmed by conducting elemental mapping on the samples using Scanning electron microscope (SEM) equipped with energy dispersive X-ray spectrometer (EDX), which was in agreement with X-ray photoelectron spectroscopy (XPS) results. Transmission electron microscope (TEM) images approximated particle sizes of the samples to be between 1.5 – 3.5 nm in diameter and this compares well with XRD analyses. Phonon quantification in TiO_2 was achieved using Fourier transform infrared (FT-IR) spectroscopy. Optical bandgap from Ultraviolet/Visible/Near-Infrared was extrapolated from Kubelka-Munk relation and the narrowing of the bandgap for the doped samples as compared to the undoped sample was observed. The photoluminescence PL study of the samples revealed two emission peaks attributed to direct band-gap and defect-related emissions.

A laser beam with 980 nm wavelength was used to irradiate the samples, and the displayed emission lines of the TiO_2: Er^{3+} in the visible region of the electromagnetic spectrum confirmed up-conversion luminescence. Enhancement of up-conversion luminescence intensity due to Yb^{3+} co-doping was observed, indicating an efficient energy transfer process from the sensitizer Yb^{3+} to the activator Er^{3+}.

Key terms

Sol-gel, annealing, TiO_2 nanopowders, optical band-gap, up-conversion luminescence, rare earth, erbium, ytterbium

Acronyms

EDX – Energy dispersive X-ray spectroscopy

FT-IR – Fourier transmission infrared spectroscopy

SEM – Scanning electron microscope

PL - Photoluminescence

TEM – Transmission electron microscope

UV/Vis/NIR – Ultraviolet-visible near-infrared spectroscopy

XPS – X-ray photoelectron spectroscopy

XRD – X-ray diffraction

Table of Contents

Chapter 1

Introduction

1.1 Background

Nanotechnology is defined as the science and technology of small things – In particular, it deals with materials, devices, and systems at the molecular level [1]. Researchers have discovered that materials at small dimensions, typically 1 to 100 nm can have distinctly different properties than their bulk counterparts: these properties include enhanced optical properties and larger specific surface area [2]. Nanotechnology is an interdisciplinary field of study that combines condensed matter physics, chemistry, and engineering – making it applicable in virtually all areas of human life [2, 3]. This technology is sought to be one of the biggest driving forces in research of materials science and economy in the 21st century and beyond [4].

In recent years, knowledge in this relatively new field of science has been growing drastically [5]. This interest has helped in enhancing the quality of ceramics, metals, polymers and biomaterials which are responsible for the emergence of advanced technologies which will have a huge impact in our everyday life [6]. In particular fabrication of nanomaterials offers exciting and intelligent approach towards creating new and advanced way to capture, store and transfer energy [6, 7]. Understanding of nanotechnology is essential for the future; therefore much work still needs to be done in this newly born field of science [5].

In materials physics, for many years much effort has been devoted to exploring the traditional luminescent materials also known as phosphors in bulk form. However recently; the synthesis of efficient luminescent materials at a nano-scale has found tremendous interest from research community globally [5, 8]. In a nano-regime, common materials display unique physical and chemical properties caused by many factors such as lower melting points, faster chemical reactions and remarkably lower resistance to electricity [9]. One of the most essential properties of nanoparticles is the increase of their specific surface area i.e. they possess a very high surface-to-volume ratio (see **Figure 1.1**).

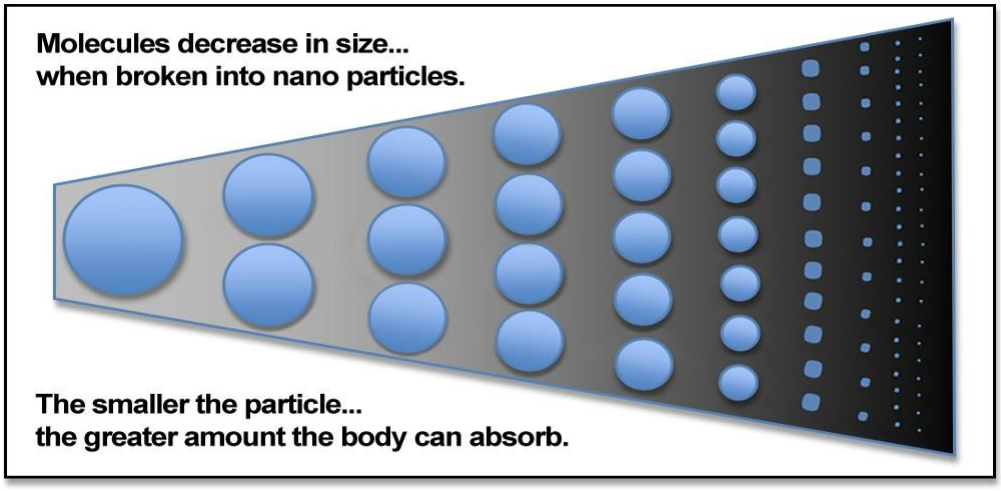

Figure 1.1: Schematic diagram of large surface-to-size ratio [10].

At a nano-scale, particles can also display fascinating size dependent features–when the diameter of the particle is decreased the band gap (E_g) is blue-shifted due to a phenomenon called quantum confinement effect [9], i.e. the energy gap of a semiconductor increases with decreasing particle size. A detailed discussion on quantum confinement effect will follow in the next chapter.

In this study, the main focus is on the synthesis and characterization of undoped TiO_2 and trivalent rare earth Er^{3+} doped and Er^{3+}-Yb^{3+}co-doped TiO_2 at a nano-scale in order to explore their unique and interesting structural and optical properties. The fascination about TiO_2 is mainly due to its non-toxicity and good stability in various environments [11]. Additionally, TiO_2 can be used as an effective photocatalyst for water and air purification [12], and for self-cleaning surfaces [12], gas sensors, optical coating and in solar cells for production of hydrogen and clean energy due to its relatively wide band gap of (3.0-3.2) eV [13]. In photovoltaic applications; TiO_2 is a promising host semiconductor for rare earth up-conversion, a process in which a light of lower energy is up-converted into a light of a shorter wavelength (higher energy), two or more low energy photons are required for this process to take place [14]. It has been proven that the above-mentioned applications of TiO_2 are highly dependent on the particle size of TiO_2 powder used in the synthesis of devices or components [15]. In line with this, the main challenge is to increase the efficiency of processes such as photo-conversion, luminescence, and extension of the spectral sensitivity of TiO_2 nanoparticles [14]. Various physical and chemical methods are available for preparation of TiO_2 based luminescent nanoparticles such as sol-gel [16], chemical vapor decomposition [17], reactive sputtering [11] and microwave assisted method [18]. Among these methods, the sol-gel route has shown to be the most preferred method due to unique advantages such as low cost [19], ease of synthesis [20], easily transferrable to industrial conditions [11] and it produces samples with high purity and good homogeneity at a nano scale [20, 21].

Doping TiO_2 with rare earth ions is a popular technique which facilitates the visible light activity of TiO_2 [22]. In 2011, Antic et al. conducted a study to investigate photoluminescence of rare earth ions doped TiO_2 nanoparticles [23].

A successful incorporation of the trivalent rare earth (RE^{3+}) ions (Eu^{3+}, Sm^{3+}, and Tb^{3+}) via hydrolytic sol-gel method was reported. They observed that band- gap energies change slightly with rare earth ion incorporation, from 3.32 eV for undoped TiO_2 to 3.15 eV, 3.25 eV, and 3.39 eV for Tb^{3+}, Sm^{3+}, and Eu^{3+} doped TiO_2, respectively. They have also reported that photoluminescence of Eu^{3+} and Sm^{3+} originated from three different sites in TiO_2 nanocrystals with one side exhibiting broad emission peaks which are ascribed to the distorted lattice site near the surface. Other two sites exhibited significantly sharper fluorescence lines which are associated with the inner lattice [23].

By doping TiO_2 with different up and down- converting rare earth ions, efficient light emitting materials can be achieved. These materials have a great possibility of replacing standard type or traditional bulk based phosphors. Thus, this study will be devoted to studying the luminescence of rare earth doped TiO_2 nanoparticles considering the advances that have been made in the past.

1.2 Problem Statement

In materials physics, for many years much effort has been devoted to exploring the traditional luminescent materials such as sulphide based phosphors [24], this fascination is attributed to their ability (in contrast to oxide materials) to provide a broad band and they also possess several characteristic properties such as color conversion and long afterglow [25]. However; it has been indicated that these materials become more unstable (due to very high electric fields needed to drive the device) and non-luminescent in the presence of residual gasses such as oxygen [26, 27].

Moreover, in recent years, the oxide based materials with nanoscopic dimensions have attracted a great deal of attention due to their intriguing properties such as high chemical and high thermodynamic stability under high current densities, high-vacuum pressures and elevated temperatures [9, 28]. Finally, oxide phosphors also tend to degrade under strong excitation or bombardment [29].

The main reason for choosing TiO_2 is its non-toxicity, low cost and good stability in various environments [11]. One of the most attractive attributes of TiO_2 nanoparticles is water-splitting ability for hydrogen production; this provides a promising method to obtain clean, low-cost and environmentally friendly fuel by solar energy [30]. But it possesses some limiting factors such as poor absorption of visible radiation (wide band gap) and rapid recombination of photo-generated electron-hole pairs [30, 31]. Applications of traditional down-conversion materials have at times been restricted due to their inability to overcome drawbacks such as photo-bleaching, high background noise from auto fluorescence, and photo damage [32, 33]. An alternative that avoids some of these limitations is near infrared to UV-Vis up-conversion materials, consequently this study is devoted to exploring doping of TiO_2 with up-converting RE ions.

New enhanced novel phosphors with high efficiency, persistent luminescence lifetime and intensity are needed for the development of various nano-technologically advancing industries. In this respect, the most important challenge in this relatively new field of study is to engineer/tune properties of these phosphors such as band gap, morphology, particle size, and concentrations in order to achieve new materials for specific desirable applications in various devices considering the advances that have been made in the past.

1.3 Study Objectives

In this study, much effort is devoted to the synthesis of undoped TiO_2 and (Er^{3+} doped and Er^{3+}/Yb^{3+} co-doped) TiO_2 nanoparticles in order to explore their structural and optical properties. In line with this, other activities include:

- To investigate the effect of introducing Yb^{3+} as a co-dopant in Er^{3+} doped TiO_2 nanoparticles.
- To study the effect of dopant concentration on the optical properties of TiO_2 nanoparticles.
- To study the surface effects (defects and vacancies) on the optical properties of TiO_2 nanoparticles, especially in comparison with reference bulk materials.
- To evaluate the properties of the prepared samples for possible applications in various devices such as solar cells, lighting, and bio-imaging devices.

Phosphors have a wide variety of applications, it is, therefore, important to extensively study their properties. In addition, a secondary objective of this study will be the development of a synthesis method as optical properties of doped phosphors predominantly arise from the dopants/impurities and the impurity sites in the host matrix which are mainly created during preparation.

1.4 Thesis Layout

- **Chapter 2** is dedicated to the literature review.
- **Chapter 3** discusses in detail a complete procedure of the synthesis and characterization of the prepared materials.
- **Chapter 4** presents the study of TiO_2: Er^{3+} nanocrystals based on their structural, elemental, morphological and optical properties.
- **Chapter 5** presents the structural and optical properties of TiO_2: Er^{3+} nanoparticles, and the effects of co-doping with Yb^{3+}.
- **Chapter 6** outlines the findings of the research and suggestions for possible future studies to be conducted based on the findings.

1.5 References

[1] Rana AK, Rana SB, Kumari A, Kiran V, *International Journal of Recent Trends in Engineering*, **2009**, 1(4), 46.

[2] http://www.nnin.org/nnin_edu.html, [Accessed 19 January 2016].

[3] Roco MC, Bainbridge WS, *Social Implications of Nanoscience and Nanotechnology, (Springer, Boston)* (**2001**), 1-2.

[4] Rogach AL, Eychmuller A, Hickey SG, Kershaw, *Reviews: Infrared emission,* **2007**, 3, 536.

[5] Dhlamini MS, *Luminescent properties of Synthesized PbS nanoparticles phosphors*, **2008**, [Ph.D. Thesis], University of the Free State, South Africa.

[6] Daoutsali E, Barke HD, Yadav OP, *AJCE,* **2014**, 4(4), 2-15.

[7] http://www.npep.co.za, [Accessed 20 January 2016].

[8] Hayle ST, Gonfa GG, *American Journal of Nanoscience and Nanotechnology,* **2014**, 2(1), 1-7.

[9] Biggs M, *Synthesis, Characterization, and Luminescent mechanism of ZnS: Mn^{2+}nanophosphor*, **2009** [MSc Thesis] University of Free State, South Africa.

[10] http://harmonyhealthproducts.com [Accessed on 23 February 2016].

[11] Gaur AM, Joshi R, Kumar M, *Deposition of doped TiO_2 thin film by sol-gel technique and its characterization: A review, world congress and Engineering* **2001**, 2.

[12] Zaleska A, *Doped-TiO_2: A review, Recent patents on engineering*, **2008**, 2,157-164.

[13] Diebold U, *Surf. Sci. Rep.*, **2003**, 48, 5.

[14] Reszvzynska J, Iwulska, Sliwinski, Zaleka A, *Physiochem. Probl. Miner. Process*, **2012,** 48(1), 201-208.

[15] Tan OK, Cao W, Hu Y, Zhu W, *Ceramics International* **30** (2004) 1127.

[16] Zhang Q.F, Park J.T, Myers X.D, Cao, G.Z, *Adv. Energy Mater.* **2011**, 1, 988-1001

[17] Choy K.L, *Prog. Mater. Sci.*, **2003**, 48(2), 57-170.

[18] Akpan UG, Hameed BH, *A Review: The advancement in sol-gel method of doped-TiO_2 photocatalysts, Appl. Catal.: General*, **2010**, 375, 1-11.

[19] http://www.uio.no/10KJM5100_2006_sol_gel_dpdf [Accessed 10 April 2014].

[20] Tang ZL, Zhang JY, Cheng Z, Zhang ZT, *Mater. Chem. Phys,* **2002**, 77, 314.

[21] Stengl V, Bakaradjiera, Murafa N, *Mater. Chem. Phys,* **2009**, 114, 217-226.

[22] Reszczy J, Grzyb T, Sobczak JW, Lisowski W, Gadza M, Ohtani B, Zaleska A, *Applied Surface Science*, **2014**, 307, 333-345.

[23] Antic Z, Krsmanovic RM, Nicolic MG, Marinovic-Cincovic M, Mitric M, Polizzi S, Dramicanin MD, *Mater. Chem. Phys*, **2012**, 135(2-3), 1064-1069.

[24] Zhang C, Lin J, *Chem. Soc. Rev.*, **2012**, 41, 7938-7961.

[25] Bem B.D, *Thermal, Structural and Luminescent Properties of Long After-Glow* Mal_xO_y*:* Eu^{2+}, Dy^{3+} *(M: Sr, Ba) Phosphors*, 2010, [Ph.D. Thesis], University of Free State, South Africa.

[26] Kabongo G.L, Luminescence investigation of zinc oxide nanoparticles doped with rare earth ions, [MSc. Thesis], **2013**, University of South Africa, South Africa.

[27] Smet PF, Moreels I, Hens Z, Poelman, *Luminescence in Sulfides: A Rich History and a bright Future*, *Materials*, **2010**, 3, 2824-2883.

[28] Pandey S, Verma P, Pandey AC, *Synthesis of highly luminescent manganese doped ZnS Nanophosphor, Nanophosphor Application Center; University of Allahabad*, **2006**, 259-261.

[29] Mhlongo GH, *Luminescence investigation of trivalent rare earth ions in sol-gel derived* SiO_2 *and ZnO co-doped* SiO_2*:* Pr^{3+}, [MSc thesis], **2011,** University of Free State, South Africa.

[30] Shon HK, Phuntsho S, Okour Y, Cho DL, Kim JB, Na S, Kim JH, *Visible light Responsive Titanium Dioxide (*TiO_2*), a review* (**2008**).

[31] Gupta SM, Triphati M, *A review of* TiO_2 *nanoparticles, Physical Chemistry*, **2011**, 56(16), 1639-1657.

[32] Chatterjie D.K, Gnanasammandhan M.K, Zhang Y, *Small*, **2010**, 6(24), 2781-2795.

[33] Chen J, Zhao J.X, *sensors*, **2012**, 12, 2414-2435.

Chapter 2

Basic Literature

Luminescent nanomaterials or nanophosphors have inspired intensive research efforts by research community globally. Nanomaterials are defined as a set of substances where at least one dimension is less than approximately 100 nm. Nanophosphors are typically comprised of a host matrix that is deliberately doped with foreign atoms or impurities. The absorption of excitation energy takes place via the host matrix or impurity ion. Furthermore, phosphors are generally characterized by the emission of light from impurity sites in the visible range (380-780) but can further be luminescent active in other spectral regions (such as ultraviolet or infrared). It has been shown in the past that phosphor materials based on rare earth ions can reduce the band gap, which results in the absorption of more visible light and improved efficiency.

In this respect this chapter will discuss the basic information on trivalent rare earth ions theory of photoluminescence (down and up conversion emissions) in the UV/Vis/NIR regime and a brief discussion on the quantum size effect and optical band-gap tuning based on rare earth ions doping, and finally the background of TiO_2 in bulk and nanoscale form and its applications will be discussed.

2.1 Luminescence

Luminescence is defined as the phenomenon that deals with the emission of electromagnetic radiations (light) in the region between UV and IR from solid materials known as phosphors, excited by some kind of external energy [1]. Luminescence can be categorized into different types depending on the excitation source; see **Table 2.1** and the main focus in this study will be on photoluminescence, so our discussion is limited to photoluminescence.

Table 2.1: The different types of luminescence.

Name	Excitation source
Photoluminescence	Light
Cathodoluminescence	Electrons
Radioluminescence	X-rays, α-, β-, or γ-rays
Thermoluminescence	Heating
Electroluminescence	Electric field or current
Triboluminescence	Mechanical energy
Sonoluminescence	Sound waves in liquids
Chemiluminescence and bioluminescence	Chemical reactions

2.1.1 Photoluminescence

Photoluminescence is divided into two categories, namely: phosphorescence and fluorescence according to time periods between absorption and emission of photons [2]. Phosphorescence is a specific type of luminescence whereby the material does not immediately re-emit the radiation it absorbs, the light emission can continue for few seconds, minutes or hours after exciting radiation has ceased, while fluorescence is a process in which emission stops suddenly after radiation has ceased [3]. Photoluminescence (PL) can be defined as a process in which an electron is elevated to higher energy upon photon absorption.

After excitation, the electron can return to the lower lying level via two possible paths; radiative decay and non-radiative decay. These two are competing processes [4]. Non-radiative decay is when an excited electron relaxes to the lower lying level by emitting phonons. In such a case, no emission is observed and absorbed energy is dissipated as heat in the system while in radiative decay, electron decays by emitting photons [4, 5]. These two processes are described in **Figure 2.1**.

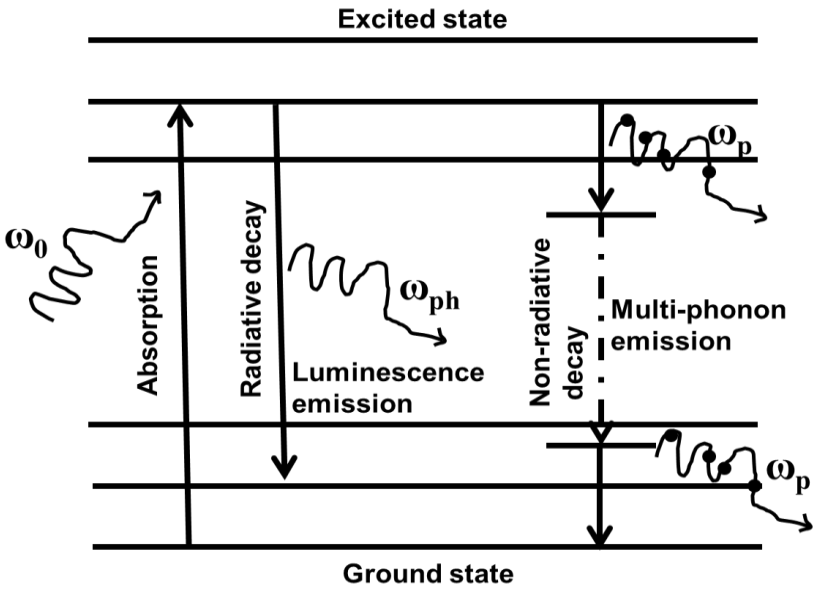

Figure 2.1: Interactions among photon, electron, and phonon: photon absorption and emission, electron excitation and decay, and phonon emission [5].

The PL process is generally classified in terms of the nature of the electronic transitions generating it. In general, PL is categorized into two distinct classes, namely; extrinsic and intrinsic luminescence [6]. Extrinsic luminescence is the phenomenon in which phonons are generated by intentionally incorporated foreign atoms or defects in the host matrix, whereas intrinsic luminescence exists in three different luminescence processes, namely; band to band luminescence, exciton luminescence and cross-luminescence [6].

2.2 Up-conversion and its mechanisms

Up-conversion is an optical process in which phosphor materials emit detectable photons of higher energy in the UV-Vis/NIR from lower-energy radiation (usually near-infrared radiation). However, for this process to occur two or more photons are required [7, 8]. The up-conversion phenomenon has been extensively studied since the mid-1960s and widely used in solar cells, lasers, sensors, optical imaging, and photodynamic therapy etc. In the field of imaging; the main advantage of up-converting materials is that they overcome the drawbacks faced by traditional down-conversion materials such as photo-bleaching, high background noise from auto fluorescence, and considerable photo damage [7, 8].

In recent years, due to the rapid development of nanotechnology; high-quality rare-earth (RE) doped up-conversion nanoparticles have been successfully synthesized [8]. Most RE ions can undergo up-conversion process; however, only a few trivalent RE ions (e.g. Er^{3+} and Tm^{3+}) have relatively efficient up-conversion [8]. Wang et al. [9] investigated the degradation of ethyl violet dyestuff using visible light in the presence of an ordinary rutile TiO_2 catalyst doped with RE up-conversion luminescent agents, in addition to the visible light photocatalytic activities of RE-doped TiO_2 nanocrystals reported by Feng et.al [10]. However, the most popular combination is the Er^{3+}/Yb^{3+} or Tm^{3+}/Yb^{3+} co-doped hexagonal $NaYF_4$ crystals, shown as materials with the highest up-conversion efficiency due to its low phonon energy [11].

In the present work, we will briefly discuss the mechanism of up-conversion phenomenon but mainly focus on Er^{3+} -doped TiO_2 nanoparticles and Yb^{3+}/Er^{3+} co-doped TiO_2 nanoparticles.

2.2.1 Up-conversion mechanisms

Different up-conversion luminescence mechanisms can take place either alone or in combination, but one is usually more dominant [12]. Up-conversion is complicated in practice, but several basic mechanisms that contribute to up-conversion emission will be discussed here.

2.2.1.1 Energy transfer up-conversion (ETU)

ETU has the highest probability and it is a far more efficient up-conversion process than ESA and was first proposed by Auzel et al. [13] and by Ovsyankin et al. [14] independently in 1966. The ETU process can be achieved by either non-radiative or radiative energy transfer between two neighboring ions. In essence, two ions undergo ground state absorption (GSA) and one ion relaxes to a lower energy level by transferring its energy to the other ion. This ion is then elevated to a higher energy level. Finally, the excited ion relaxes to the ground state under the emission of a photon [5]. ETU can occur between the same type of rare-earth ions (e.g. two erbium ions, or between different types of ions (e.g. erbium and ytterbium ions)) [5]. An overview of the ETU up-conversion mechanism based on isolated energy levels is given in **Figure 2.2**.

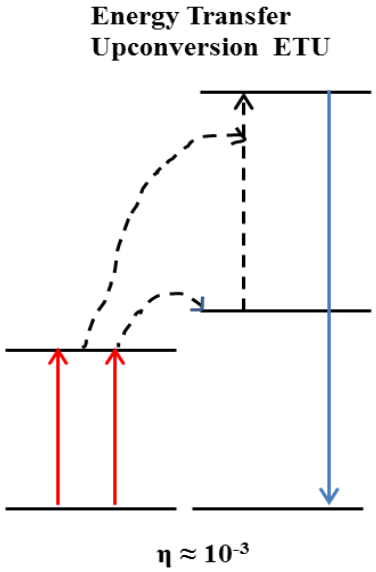

Figure 2.2: Energy transfer up-conversion mechanisms and estimated relative efficiencies [13].

2.2.1.2 Excited state absorption (ESA)

Excited state absorption ESA is the next most efficient process; it involves a multi-step excitation by sequentially absorbing one or more photons from the ground state to intermediate reservoir stage [8, 15]. Note that ESA is more precisely described as GSA-ESA process in which one ion or electron in ground state absorbs one photon (GSA), this ion is then elevated to higher energy level, after sequentially absorbing the second photon (ESA), it can jump to even higher energy level, consequently emitting higher energy photon as it relaxes back to the ground state [8, 13, 15]. This process gave birth to the whole field of up-conversion in ion-doped systems since its introduction by Bloembergen in 1959 when he proposed sequential absorption with the levels of a given ion in a solid [16]. An overview of the ESA up-conversion mechanism based on isolated energy levels is given in **Figure 2.3**.

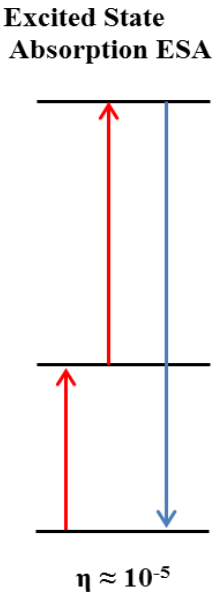

Figure 2.3: Excited state absorption up-conversion mechanism and estimated relative efficiencies [13].

2.2.1.3 Co-operative up-conversion

Co-operative up-conversion is the least efficient of the three processes [15]. It is about 3-5 orders of magnitude less effective than ETU [17]. Co-operative up-conversion is considered practically feasible when ETU cannot take place and it is likely to take place with clusters since it is a process involving co-operative pair states [15, 17]. An overview of the Co-operative up-conversion mechanism based on isolated energy levels is given in **Figure 2.4**.

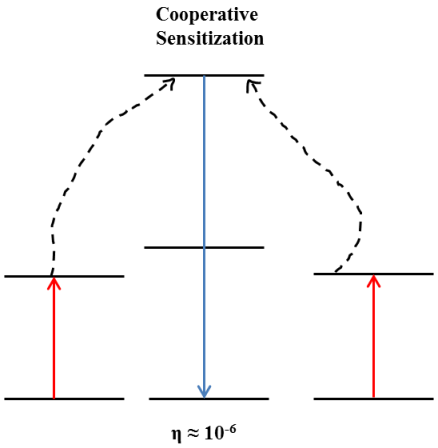

Figure 2.4: Co-operative up-conversion mechanism and estimated relative efficiencies [13].

2.3 Trivalent rare earth (RE) ions

Lanthanide ions also referred to as rare earth ions with inclusion of scandium and yttrium have attracted considerable attention from renowned scientists globally for more than two centuries now. This fascination dates back to the 1880s due to the distinct properties of rare earth ions and the fact that very little was known about these metals from the 'missing' block of the periodic table. The most intriguing feature of rare earth ions is their unique luminescence properties. In the 1950s and 1960s, research on rare earth doped II-VI compounds was intensive in an effort to develop efficient phosphor materials for industrial exploitation.

A new impetus started in the mid-1970s when renowned scientists Soini and Hemmilia [18] proposed rare earth luminescent probes for time-resolve immunoassays. This became a starting point of the present numerous bio-applications based on optical properties of rare earths. Nowadays the role of rare earth doped phosphors are extensive and rapidly growing and it has led to broad industrial exploitation in the fields such as bio-analysis, lasers, illumination and displays [6, 18].

The rare earth doped materials are of crucial importance in the nanotechnology industry. In 1968, Dieke and co-workers investigated and tabulated **(Figure 2.5)** the energy levels of the lanthanide ions in a range of crystalline materials and the rare earths have widely been used as activators in phosphors for several decades [19].

The rare earth ions, hereafter RE^{3+} includes 15 lanthanide elements (Z=57 through 71) and these rare earth ions possess the electronic [Xe] $4f^n$ configurations (n = 0-14) [6, 20] **(see Table 2.2)**. This makes RE ions particularly unique due to their ability to generate a broad variety of electronic levels, given by $\frac{14!}{n!(14-n)!}$ [21].

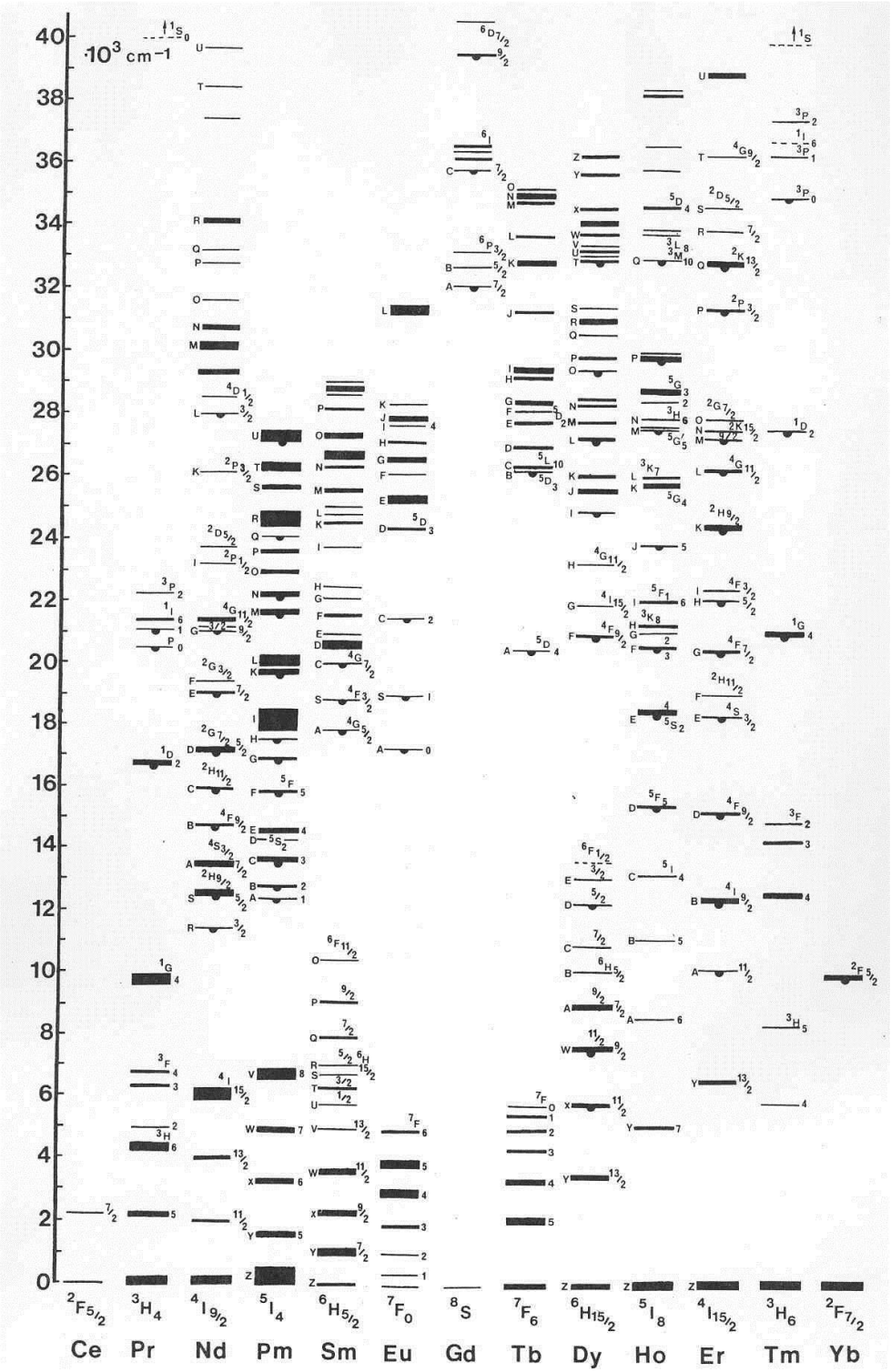

Figure 2.5: Energy-level diagram for trivalent lanthanide rare earth ions in lanthanum chloride ($LaCl_3$) [6].

Table 2.2: Electronic structure of RE^{3+} ions.

Element	Symbol	Atomic No. (Z)	Configuration Ln^{3+}	Ground state Ln^{3+}
lanthanum	La	57	[Xe]	$^1S_0$
cerium	Ce	58	[Xe] $4f^1$	$^2F_{5/2}$
praseodymium	Pr	59	[Xe] $4f^2$	$^3H_4$
neodymium	Nd	60	[Xe] $4f^3$	$^4I_{9/2}$
promethium	Pm	61	[Xe] $4f^4$	$^5I_4$
samarium	Sm	62	[Xe] $4f^5$	$^6H_{5/2}$
europium	Eu	63	[Xe] $4f^6$	$^7F_0$
gadolinium	Gd	64	[Xe] $4f^7$	$^8S_{7/2}$
Terbium	Tb	65	[Xe] $4f^8$	$^7F_6$
Dysprosium	Dy	66	[Xe] $4f^9$	$^6H_{15/2}$
Holmium	Ho	67	[Xe] $4f^{10}$	$^5I_8$
Erbium	**Er**	**68**	**[Xe] $4f^{11}$**	**$^4I_{15/2}$**
Thulium	Tm	69	[Xe]$4f^{12}$	$^3H_6$
Ytterbium	**Yb**	**70**	**[Xe] $4f^{13}$**	**$^2F_{7/2}$**
Lutetium	Lu	71	[Xe] $4f^{14}$	$^1S_0$

One of the attractive attributes of rare earths is that their energy levels are well defined leading to line-like emission due to the shielding of the 4f orbitals by the filled $5s^25p^6$ sub-shells [6, 20]. For this reason, the RE ions can be used in all sorts of host materials as compared to main group elements and transition metals [6]. In most cases, the emission of absorbed excitation occurs via the rare earth ion resulting in sharp f-f emission lines in which the emission color is characteristic of the rare earth ion emitting it [22]. (**See Figure 2.6)**

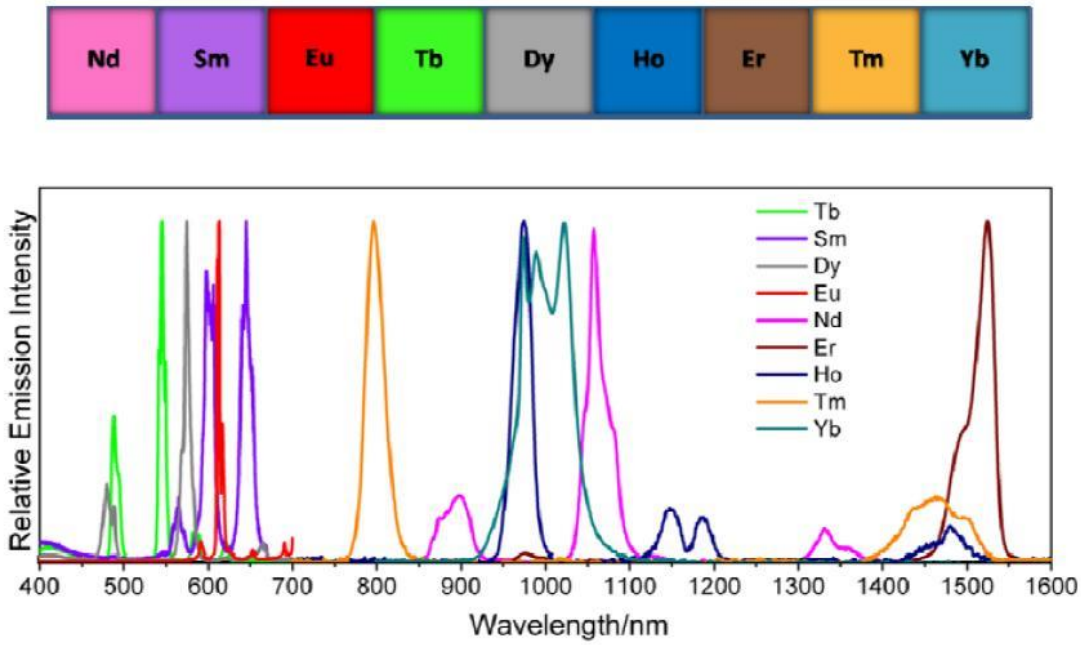

Figure 2.6: Luminescent rare earth cations and their characteristic emission bands [22, 23].

Except for the 4f-4f transitions in rare earth ions, there are other two types; 4f-5d optical transitions and charge-transfer transitions (rare earth to host/host to rare earth) [5]. All trivalent rare earth ions with exception of La^{3+} and Lu^{3+} are luminescent and their emission of the excited electron via f-f transitions cover the entire spectrum from UV (Gd^{3+}) to visible (e.g. Pr^{3+}, Sm^{3+}, Eu^{3+}, Tb^{3+}, Dy^{3+}, Tm^{3+}) and NIR (e.g. Pr^{3+}, Nd^{3+}, Ho^{3+}, Er^{3+}, Yb^{3+}) ranges [20]. There are two trivalent rare earth ions that were used in this study; these are Erbium (Er^{3+}) and Ytterbium (Yb^{3+}). These rare earth ions are doped into a TiO_2 host and the detailed discussion for choosing these ions will follow.

2.3.1 Erbium

Erbium, as an element is a member of the lanthanide rare earth series which possesses [Xe] $6s^2f^{12}$ ground state electron configuration. However, Er has particularly unique up-converting properties in its trivalent charge, having lost its two 6s electrons and one 4f electron, [Xe] $4f^{11}$ [5].

The rare-earth ion Er^{3+} can act as an up-converter by converting two near-infrared (NIR) photons into one visible photon. The process of up-conversion occurs when Er^{3+} is doped into a host material. Accordingly, Er^{3+} is doped into TiO_2 via a sol-gel method [24] to obtain a high conversion of NIR light into visible light [25].

The high energy light emitting states can be populated by multiple excitation steps as shown in the Dieke diagram on **Figure 2.5** [5]. Erbium provides adequate up-conversion properties due to its ground state absorption at about 1500 nm ($^4I_{15/2} \rightarrow {}^4I_{13/2}$) [15]. One of the most attractive attributes of erbium in up-conversion processes is the location of the energy levels $^4I_{13/2}$, $^4I_{9/2}$, $^2H_{11/2}/^4S_{3/2}$, and $^2H_{9/2}$ in nearly equal distances matching the excitation wavelength of the ground state [15]. Furthermore, by using different excitations sources different intermediate states are employed. Some excitation paths in Er^{3+} are illustrated in **Figure 2.7** for 1500 nm excitation.

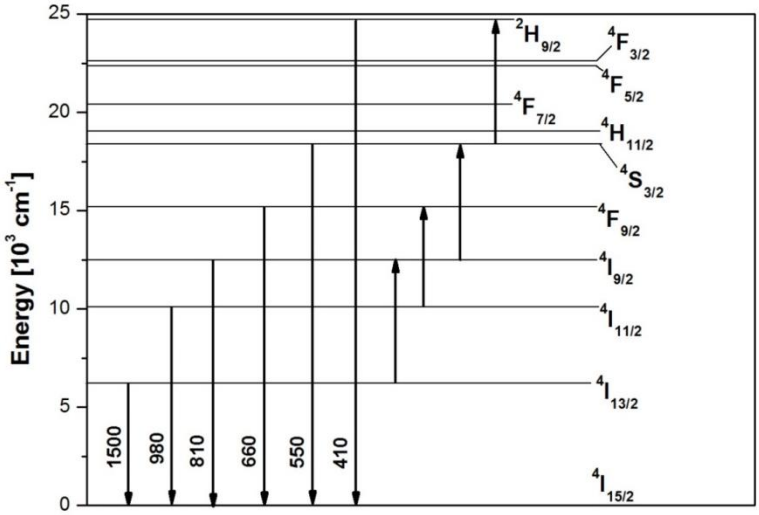

Figure 2.7: Energy level of a free trivalent erbium ion [15].

The upright arrows represent the transitions involved in up-conversion processes occurring under the excitation wavelength of 1500 nm.

Three different up-conversion processes can occur under excitation at about 1500 nm, namely Ground State Absorption (GSA), Excited State Absorption (ESA), and Energy Transfer-based up-conversion (ETU) [15]. There is an increasing demand for the properties of erbium as an up-converter. However, a comparison is difficult since the results are mostly presented in arbitrary units. A wide variety of comparative measurements on erbium-doped materials in terms of efficiency have been undertaken by many researchers in the past [15].

Ohwaki and Wang et al. [26] conducted a study of erbium doped ($BaCl_2$, YBr_3, YI_3, and YF_3) host materials, they reported that $BaCl_2$: Er^{3+} showed the highest upconversion efficiency, followed by YBr_3 and YI_3 and the lowest upconversion efficiency was found in YF_3 host material. These findings were found to be consistent with the studies conducted by van der Ziel et al. [27].

Prior studies have shown that room temperature emission from erbium in oxide-based hosts becomes diminished at high erbium concentration [28]. However, Park et al. [29] reported a successful incorporation of relatively high erbium concentrations in SiO_2 waveguide structures in which, high gains and intense PL signals were observed. The above-mentioned considerations, therefore, inspired the present strategy of varying the concentration of erbium in order to explore its effect on the optical properties of TiO_2 host material. In most cases, due to less absorption; the up-conversion process has a low efficiency and consequently this study will also explore the method of co-doping with the sensitizer (Yb^{3+}) for enhancing the up-conversion luminescence. Details of co-doping will follow.

2.3.2 Co-doping with Yb^{3+}

In most cases, the up-conversion process has a low efficiency. However, much larger conversion efficiencies can be achieved by co-doping with another rare earth ion [30].

In this study, we investigate the up-conversion characteristics of TiO_2 nanoparticles doped with rare earth ion Yb^{3+}-Er^{3+} pair at different relative concentrations to yield the highest up-conversion luminescence emission output [25]. Ytterbium possesses a ground state electron configuration of [Xe] $6s^2 4f^{14}$. In its trivalent form, the configuration becomes [Xe] $4f^{13}$ upon losing 2 electrons from 6s and 1 electron from 4f orbitals. It also has a very simple two-level energy system, consisting of one excited energy level $^2F_{5/2}$ around 980 nm [5]. Yb^{3+} has a larger and spectrally broader absorption cross section than Er^{3+} [31]. To enhance the absorption of Er^{3+}, Yb^{3+} is used as a sensitizer whereby Yb^{3+} absorbs and transfers the energy of Er^{3+}, in which the emission occurs [15]. The $^2F_{5/2}$ level of Yb^{3+} has a long lifetime and it is also resonant with the $^4I_{11/2}$ level of Er^{3+} (**Figure 2.8**) [25]. Johannsen et al. [5] reported the enhancement of 109 times for green emission and 50 times for red emission by co-doping with Yb^{3+} into TiO_2: Er^{3+} thin films.

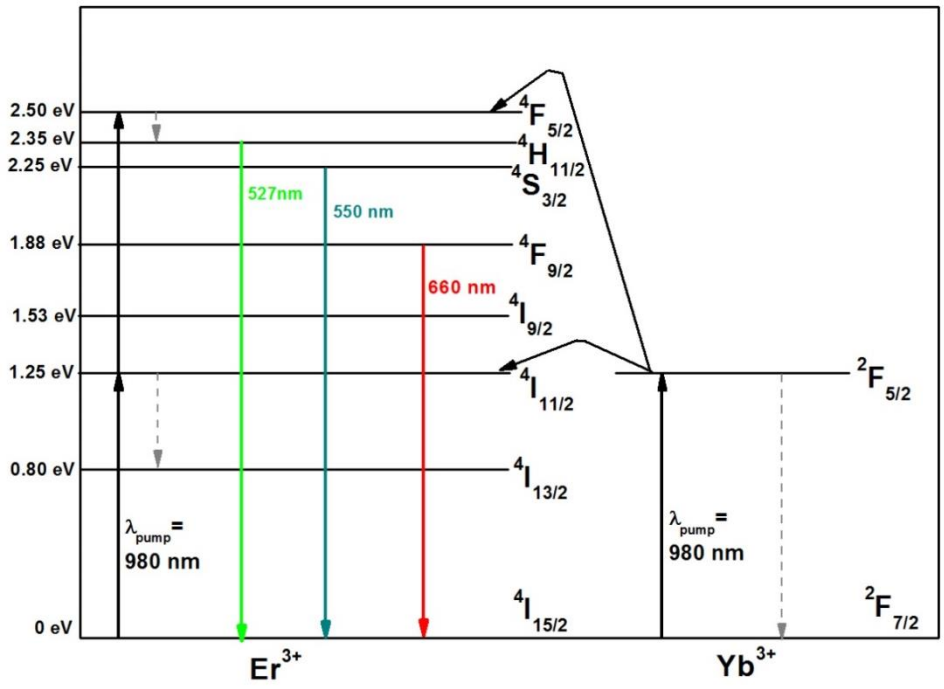

Figure 2.8: Up-conversion luminescence mechanism in the visible region from energy levels of Er^{3+} upon laser excitation into absorption band of Yb^{3+} [5].

2.4 TiO_2 as a host matrix

In recent years, several investigations of host materials doped with rare earth ions have been carried out [15]. It has been reported that the host lattice plays a vital role in the up-conversion luminescence efficiency [7]. Therefore it is crucial to choose a good combination of the host lattice and dopant ions [7]. Ideally, the host material is required to have good lattice matching with the dopant ions [17] and the appropriate host material should have low lattice phonon energies (high phonon frequencies of the host lattice lead to non-radiative relaxation) [8, 17]. Other conditions that the host material should fulfill include chemical stability, biocompatibility of materials, and the good interionic distance between the sensitizer and activator in the host lattice [7, 8, 17]. Naturally, TiO_2 exists in three different crystallographic forms- anatase, rutile, and brookite [33]. These are shown in **Figure 2.9**.

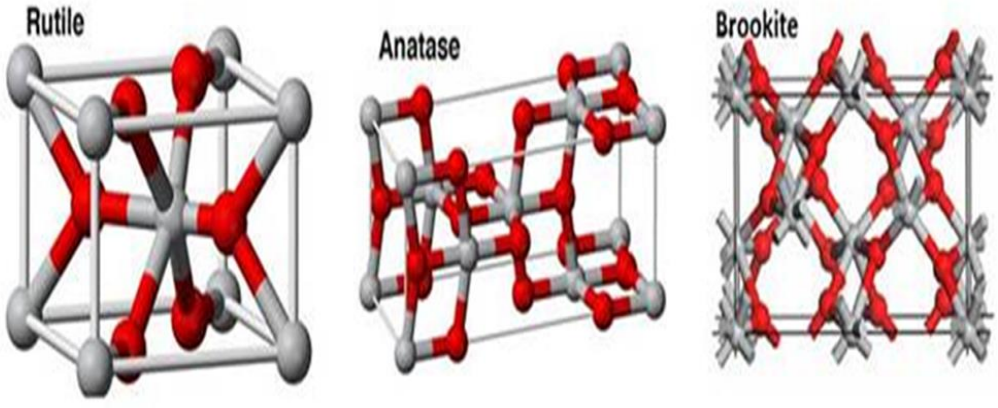

Figure 2.9: Various crystallographic structures of TiO_2 [33].

Among them, rutile and anatase are of engineering importance due to their unique properties [32], consequently, they have been widely studied. Brookite is the least stable and it is rarely studied due to its complicated structure and difficulties in sample preparation [34].

The anatase and rutile phases both have a tetragonal crystal structure, whereas brookite phase has an orthorhombic structure [35]. However, anatase phase is stable at lower temperatures and has a refractive index of 2 with optical energy band gap of 3.2 eV (380 nm), rutile is a high-temperature stable phase and has an optical energy band gap of 3.0 eV (415 nm) [36].

In this study, TiO_2 is selected as the host lattice due to its relatively low phonon energy of 639 cm^{-1} for anatase and 612 cm^{-1} for rutile [37, 38]. Another contributing factor towards the selection of TiO_2 as a host is that it has been extensively studied owing to its wide spectrum of applications in virtually all areas of science and technology [5], and it is a cheap non-toxic material [5, 17] with high photochemical stability [17]. A desired application of TiO_2 is highly dependent on a specific feature like crystallographic structure, particle morphology [35], surface state and particle size [39]. In a nano regime; TiO_2 provides a large-scale surface with broad band gap due to the quantum size effect of nanoparticles [40]. This quantum size effect is illustrated in **Figure 2.10**.

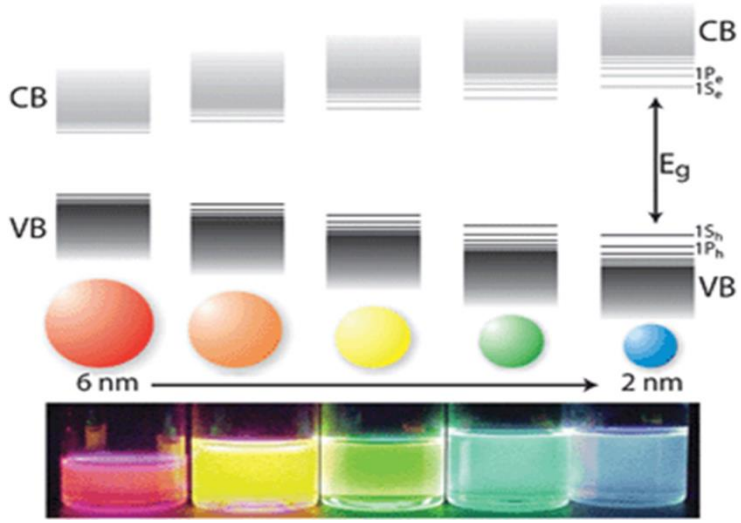

Figure 2.10: Size dependence of the band gap [41].

2.4.1 Quantum size effect

Quantum size effect also known as quantum confinement effect is arguably the most famous phenomenon in the "nano world". In essence, this quantization effect occurs when the particle dimension of a semiconductor is near the Bohr exciton radius of the bulk semiconductor [42]. In general, Bohr radius which is the distance between the electron and the hole is given by:

$$a_B = \varepsilon \frac{m}{m^*} a_0 \qquad (2.1)$$

Where ε is the optical dielectric constant, m and m^* are the mass of the electron and the mass of the particle, respectively and a_0 is the Bohr radius of the hydrogen atom [43]. When the particle size of the semiconductor decreases from its bulk to that of Bohr radius, a collapse of continuous energy bands of a bulk material into discrete energy bands occurs, leading to spatial confinement of the excitons in a potential well i.e. excitons do not experience the delocalization that occurs in the bulk phase as a result the band gap of the semiconductor particle increases with decrease in particle size [44, 45].

The exciton Bohr radius of TiO_2 is reported to be only 1.5 nm, making it difficult to undergo quantum confinement effect [46]. However, there have been reports of a blue shift in the absorption edge for a very small TiO_2 nanoparticles attributed to other reasons other than the quantum confinement effect such as multi-exciton generation (MEG) [46].

2.4.2 RE^{3+} ions and band-gap tuning

One of the most effective ways for band-gap tuning for TiO_2 particles is an incorporation of rare earth ions into its lattice. The present study will be centered on UV/Vis/NIR luminescence excitation spectra of Er^{3+} doped into TiO_2 lattice as an activator ion and Yb^{3+} as a sensitizer.

To investigate the role of these dopants in the luminescence process, knowledge of their optical properties such as optical band-gap is crucial for an improved understanding of the overall system [48]. It has reported that absorption edge of TiO_2 shifts towards lower wavelengths (blue shift) after a successful incorporation of Er^{3+} ions in its lattice, this behavior is attributed to the creation of some intermediate energy levels within the band gap of TiO_2 resulting in the band-gap narrowing [48].

2.5 Applications of TiO_2

One fundamental question to be asked is how might this study improve our lives? We believe that the results of this study will have an overwhelming contribution to the development of various fields in the advancing nanotechnology industry and can also be used in our daily life. Low cost and efficient lanthanide activated TiO_2 nanophosphors produced from this study can be applied in the following fields:

- **Materials:** Protective nano-paint for cars and buildings (water, dirt, and chipping resistant) [49].
- **Water:** For purification, disinfection, and filtration solutions [50].
- **Health Care:** chemical and biological sensors, drugs and delivery devices [7, 8].
- **Environment:** Photocatalyst-equipped air conditioners and interior air cleaner in factories [50].
- **Energy:** Cheap and clean energy (solar cells and batteries) [5].
- **Technology:** Better data storage and computation [51].

2.6 References

[1] Bose H.N, *Indian. J. Hist. Sci.*, **1992**, 27(4), 409-420.

[2] Biggs M, *Synthesis, Characterization, and Luminescent mechanism of ZnS: Mn^{2+} nanophosphor*, [MSc. Thesis], **2009**, University of Free State, South Africa.

[3] Dhlamini M.S, *Luminescent properties of synthesized PbS nanoparticle phosphors*, [Ph.D. Thesis], **2008**, University of the Free State, South Africa.

[4] Mhlongo G.H, *Luminescence investigation of trivalent rare earth ions in sol-gel derived SiO_2 and ZnO co-doped SiO_2: Pr^{3+}*, [Ph.D. Thesis], **2011**, University of the Free State, South Africa.

[5] Johannsen S.R, *Up-conversion of near-infrared light through Er doped TiO_2, and the effects of plasmonics and co-doping with Yb*, [Ph.D. Thesis], **2015**, University of Aarhus, Denmark.

[6] Kabongo G.L, *Luminescence investigation of zinc oxide nanoparticles doped with rare earth ions*, [MSc. Thesis], **2013**, University of South Africa, South Africa.

[7] Chatterjie D.K, Gnanasammandhan M.K, Zhang Y, *Small*, **2010**, 6(24), 2781-2795

[8] Chen J, Zhao J.X, *sensors*, **2012**, 12, 2414-2435.

[9] Wang J, Zhang G, Zhang Z, Zhang X, Zhao G, Wen F, Pan Z, Li Y, Zhang P, Kang P, *Water Res.*, **2006**, 40, 214.

[10] Feng G, Liu S, Xiu Z, Zhang Y, Yu J, Chen Y, Wang P, Yu X, *J. Phys. Chem. C.*, **2008**, 112, 13692.

[11] Heer S, kompe K, Gudel H.U, Haase M, *Adv. Mater.*, **2004**, 16, 2102-2105.

[12] Bunzli J-C, Chauvin A-S, *Lanthanides in solar energy conversion, Handbook on the physics and chemistry of rare earths*, **2014**, Vol. 44, Elsevier B.V.

[13] Auzel F, *Acad. Sci.*, **1966**, 262, 1016-1019.

[14] Ovsyankin V.V, Feofilov P.P, *JE. TP. Lett.*, **1966**, 3, 494-497.

[15] Strümpel C, *Application of erbium doped up-converters to silicon solar cells*, [Ph.D. Thesis], **2007**, University of Konstanz, Germany.

[16] Bloembergen N, *Phys. Rev. Lett.*, **1959**, 2, 84-85.

[17] Lui H, *Advancing upconversion emissions for biomedical imaging*, [Ph.D. Thesis], **2014**, University of Lund, Sweden.

[18] Wolfbeis O.S, Hanninen P, Harma H, *Lanthanide luminescence: Photophysical, Analytical, and Biological Aspects*, Springer series on fluorescence 7.

[19] Kenyon A.J, *Recent developments in rare-earth doped materials for optoelectronics progress in quantum electrons*, **2002**, 26, 225-228.

[20] Svetlana V.E, Bunzli J-C. G, *Chem. Soc. Rev.*, **2010**, 39(1), 1-380.

[21] Binnemans K, Gorller-Walrand C, *Chem. Phys. Lett.*, **1995**, 235, 163-174.

[22] Petroud S, Cohen S.M, Bunzli J-C. G, Raymond K.N, *J. Am Chem. Soc.* **2003**, 125(44), 13324-5.

[23] Zhang J.P, Badger P.D, Gerb S.J, Petroud S, *Angew. Chem. Intl. Ed. Engl.* **2005**, 44, 2508.

[24] Trupte T, Green M.A, Würfel P, *J. Appl. Phy.*,**2002**, 92(7), 4117-4122.

[25] de Wild J, Merjerink A, Rath J.K, van Sark W.G.J.H.M, Schropp R.E.I, *Energy Environ. Sci.*, **2011**, 4(12), 4835-4848.

[26] Ohwaki J, Wang Y, *J. Appl. Phys.*, **1994**, 33(2), 334-337.

[27] van der Ziel J, van Uitert L.G, Grodkiewicz W, Mikulyak R.M, *J. Appl. Phys.*, **1986**, 60(12), 4262-4267.

[28] Abedrabbo S, Mohammed Q, Fiory A.T, *Appl. Surf. Sci.*, **2009**, 225(8), 4503-4511.

[29] Park O.H, Seo S.Y, Jung J.I, Bae J.Y, Bae B.S, *J. Mater. Res.*, **2003**, 18(5), 1039-1042.

[30] van Stark W.G.H.M, Meijerink A, Schropp R.E.I, *Solar spectrum conversion for photovoltaics using nanoparticles in third generation photovoltaics*, Fthenakis' V, Editor., **2012**, In Tech.

[31] Strohhofer C, Polman A, *Opt. Mater.* **2003**, 21, 705-712.

[32] Dubrovinsky L.S, Dubrovinskaia N.A, Swamy V, *Nature,* **2001**, 410, 653.

[33] http://en.wikipedia.org/wiki/Rutile [Accessed 18 February 2016].

[34] Hu W.B, Li L.P, Li G.S, Tang C.L, Sun L, *Crys. Growth Des.* **2009**, 9, 3676-3682.

[35] Mo S.D, Ching W, *Physical Rev. B.*, **1995**, 51(19), 13023-13032.

[36] Thamaphat K, Limsuwan P, Ngotawornchai B, *Nat. Sci.*, **2008**, 42, 357-361.

[37] Bahtat A, Bouazaoui M, Bahtat M, Garapon C, Jacquier B, Mugnier J, *J. Non-crystalline Solids.*, **1996**, 202, 16-22.

[38] Chen S.Y, Ting C.C, Hsieh W.F, *Thin Solid Films,* **2003,** 434(1-2), 171-177.

[39] Ramakrishna G, Ghosh H.N, *Langmuir,* **2003**, 19, 505-508.

[40] Hoffmann M.R, Martin S.T, Choi W, Bahnemann D.W, *Chem. Rev.*, **1995**, 95, 69

[41] http://www.philips.com [Accessed 10 December 2015].

[42] Zhao X, Wei C.M, Chou M, *Phys. Rev. Lett.* **2004**, 92, 236805.

[43] Yoffe A.D, *Adv. Phys.* **1993**, 42, 173.

[44] Miller D.A.B, Chemla D.S, Damen T.C, Gossard A.C, Wiegmann W, Wood T.H, Burrus C.A, *Phys. Rev. Lett.* **1984**, 53, 2173.

[45] Lin H, Huang C.P, Li W, Ni C, Ismat Shah S, Yao-Hsuan T, *App. Catal. B: Environmental.* **2006**, 68, 1-11.

[46] Balkus K.J, *New and Future Developments in Catalysis*, Elsevier Inc. Chapters, **2013**.

[47] Krupa J.C, Gerard I, Mayolet A, *ACTA PHYSICA POLONICA A*, **1993**, 84(5), 843-848.

[48] Ravaro L.P, Morais E.A, Scalvi L.V.A, Siu Li M, *ceramica*, **2007**, 53, 187-191.

[49] Roco M.C, Bainbridge W.S, *Social Implications of Nanoscience and Nanotechnology*, (Springer, Boston), **2001**, 1-2.

[50] Diebold U, *Surf. Sci. Rep.*, **2003**, 48, 5.

[51] http://www.npep.co.za [Accessed 20 January 2016].

Chapter 3

Synthesis and Research Techniques

3.1 Introduction

This chapter introduces in detail a complete procedure utilized for synthesis and characterization of as-prepared and calcined nano-sized TiO_2 doped with erbium and erbium-ytterbium pair via sol-gel method. Physical properties of these materials were investigated by a number of experimental techniques in order to extract their structural and luminescence information. The techniques used include X-ray powder diffractometer (XRD), X-ray photoelectron spectroscopy (XPS), Fourier transform infrared spectroscopy (FTIR), scanning electron microscopy (SEM), energy dispersive spectroscopy (EDS), transmission electron microscopy (TEM), ultraviolet-visible-near infrared spectrophotometer (UV/Vis/NIR), and Fluorolog spectrometer. X-ray diffraction patterns were acquired at room temperature using the Smartlab X-ray diffractometer (Rigaku) using CuKα (λ = 1.5406 Å) from 10° to 90°. A Perkin Elmer Phi 5600 ESCA system has been used for XPS analysis to collect and analyze ejected photoelectrons to produce a spectrum of emission intensity versus electron binding energy. FT-IR spectra were taken using a Perkin-Elmer instrument from 550 to 4000 cm^{-1}. Scanning electron microscopy (SEM) was used to study the surface morphology of the powders, and their chemical compositions were determined using Energy dispersive spectroscopy (EDS). TEM spectroscopy was employed to assess the particle size of the samples.

The reflectance characteristics of the powders were determined at room temperature using the 1050 UV-Vis-NIR spectrophotometer (Perkin Elmer) equipped with an integrating sphere. A continuous laser beam of 980 nm was used to excite the samples at room temperature using Fluorolog spectrometer (Jobin Yvon), and the emission was collected from 400 to 800 nm with a photomultiplier tube to investigate up-conversion properties of the samples.

3.2 Sol-gel synthesis method

Numerous methods of fabrication such as chemical vapor deposition (CVD) [1], thermal decomposition and sol-gel have been developed and applied in many applications in science and technology [2]. Among these methods, the sol-gel process offers many advantages such as ease of synthesis, easy control, better homogeneity [3], and production of high chemical purity powder [4]. In general, sol-gel process involves the evolution of inorganic networks through the formation of colloidal dispersions (sols) and the conversion of the sols to form viscous gels (sol-gel transition) [5].

A typical sol-gel process is better defined as a wet chemical route for synthesis of solid materials such as metal oxides from solution-state precursors [6]. Traditionally, the precursor is subjected to a series of hydrolysis and polymerization (condensation) reactions to form a colloidal suspension (sol) [6]. The sol can be processed further to create materials in different forms. Additionally, processing conditions such as chemical concentration, the pH, peptization time, calcinations time and temperature greatly influence the particle size and phase purity of the final product [7]. In recent years, the use of the sol-gel method has been a subject of extensive scientific interest for making advanced materials and for designing devices with specific properties [8]. An overview of the sol-gel products is presented in **Figure 3.1**.

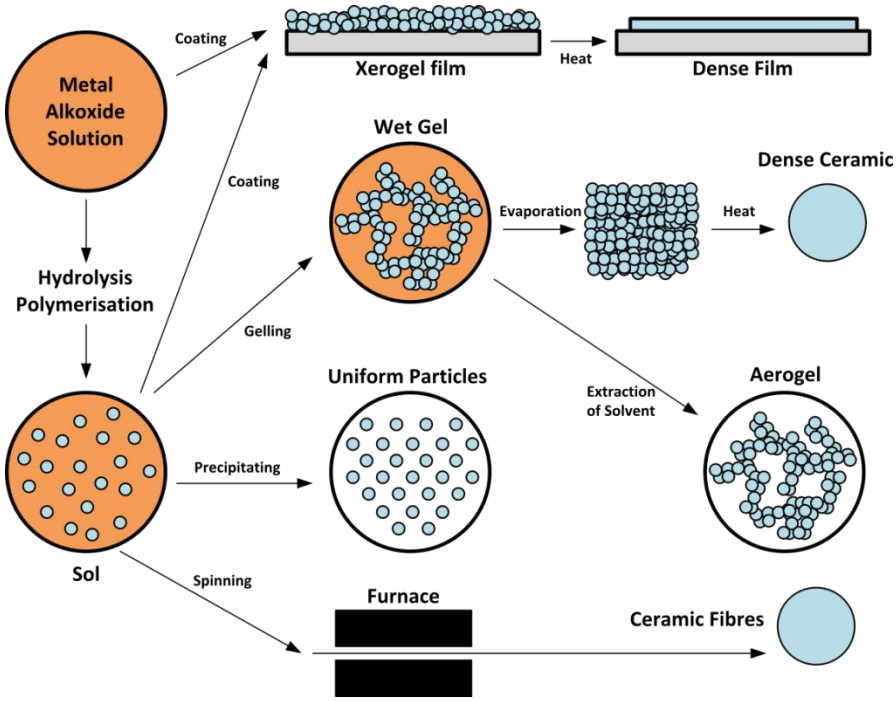

Figure 3.1: An overview of products prepared by sol-gel methods [9].

3.2.1 Starting materials used

Details of the purity and source of the starting materials used in this study are shown in **Table 3.1**. Titanium isopropoxide (TTIP) is commonly used as a precursor for the preparation of TiO_2 due to its higher absorption range in the UV range [10], high vapor pressure, noncorrosive by-products, and high-cost efficiency compared to other metal organic precursors [11]. However there are other precursors as well such as $TiCl_4$ and tetra-n-butyl-titanate etc. consequently in our study TTIP solution of 0.96 g/cm^3 in density was used as a precursor. The chemical structure of TTIP is shown in **Figure 3.2**.

Table 3.1: Raw materials used in the experiments.

Chemical Name	Molecular Formula	Purity	Company
Titanium (IV) tetraisopropoxide	$Ti[OCH(CH_3)_2]_4$	99%, solution	Sigma Aldrich, SA
Isopropanol	$CH_3CH(OH)CH_3$	70%, solution	Sigma Aldrich, SA
Deionized water	H_2O	-	Sigma Aldrich, SA
Erbium (III) nitrate pentahydrate	$Er(NO_3)_3 \cdot 5H_2O$	99%, powder	Sigma Aldrich, SA
Ytterbium (III) nitrate pentahydrat	$Yb(NO_3)_3 \cdot 5H_2O$	99%, powder	Sigma Aldrich, SA

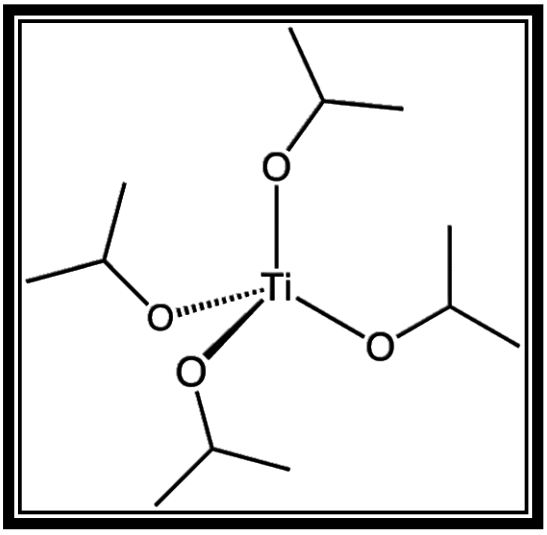

Figure 3.2: Chemical structure of TTIP [12].

3.2.2 Synthesis of undoped, Er^{3+} doped and Er^{3+}/Yb^{3+} co-doped TiO_2

In this study, TiO_2 and TiO_2: RE^{3+} (RE=Er^{3+} and Er^{3+}/Yb^{3+}) were prepared via sol-gel method using starting materials shown in **Table 3.1**. In a typical procedure; 15 ml of TTIP was added to 100 ml of isopropyl alcohol and was agitated at room temperature for 10 mins. 10 ml of deionized water was added to the mixed solution for hydrolysis reaction.

The mixture was then agitated continuously for 2 hours. Now the mixture formed a gel, which was filtered, washed and dried after aging for 24 hours. For preparation of Er^{3+} doped and Er^{3+}/Yb^{3+} co-doped TiO_2, similarly the above experimental procedure was followed, except that required amounts of $Er(NO_3)_3 \cdot 5H_2O$ and $Yb(NO_3)_3 \cdot 5H_2O$ corresponding to 1, 3, 6, 8, 10, and 12 mol% doping level were first added to the deionized water and then added into Titanium precursor solution. The pH of all the mixed solution was maintained in the range of 6-7. Oxides are generally formed during hydrolysis reaction according to the following overall reaction:

$$\mathbf{Ti[OCH(CH_3)_2]_4 + H_2O \leftrightarrow TiO_2 + 4C_3H_7OH} \qquad \mathbf{3.1}$$

A flow diagram for the preparation of TiO_2 and TiO_2: RE^{3+} nanoparticles is shown in **Figure 3.3**. The as-prepared samples were calcined at 400 °C for 2 hours in a furnace in air to produce undoped, Er^{3+} doped and Er^{3+}/Yb^{3+} co-doped TiO_2 nanopowders.

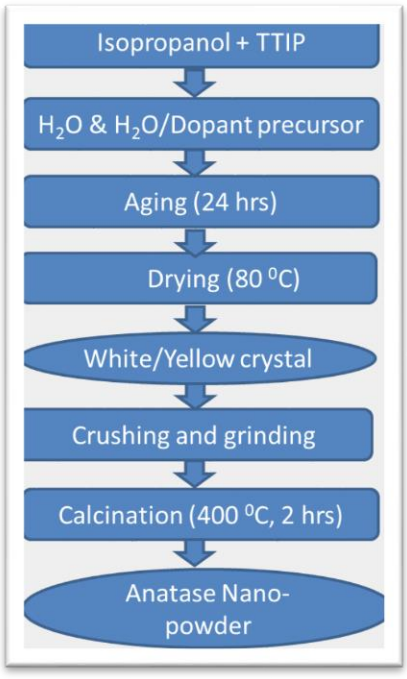

Figure 3.3: Flowchart depicting preparation of TiO_2 and TiO_2: RE^{3+} nanopowders via sol-gel process.

3.3 Characterization Techniques

3.3.1 X-ray Diffraction (XRD)

X-ray diffraction patterns, phase characterization and the estimation of crystalline sizes of synthesized powder samples were acquired by using Smartlab X-ray diffractometer (Rigaku) from the University of South Africa (UNISA). The XRD is a rapid non-destructive analytical technique primarily used for the identification of crystalline materials which is primarily used to provide information on unit cell dimensions [13]. Typically, an X-ray diffractometer is comprised of three basic elements: an X-ray tube, a sample holder, and an X-ray detector. A diffraction pattern is produced when a crystalline material is bombarded with a collimated beam of X-rays generated by a cathode ray tube. As the sample and detector are rotated, the intensity of the diffracted X-rays is measured as a function of diffraction angle 2θ and the specimen's orientation. A constructive interference occurs when the geometry of the incident X-rays bombarding the sample satisfies the Bragg equation. When this condition is satisfied then a peak in intensity occurs [14]. Bragg's law is represented by the following equation:

$$n\lambda = 2d \sin\theta \qquad 3.2$$

Where n is diffraction series, θ is a diffraction angle, λ is the wavelength of X-ray, and d is an inter-planar distance. Finally Suryanarayana et al. [15] proposed that broadening of X-ray diffraction peaks can be attributed to small crystallite size and lattice strain. **Figure 3.4** presents the basic principle of the XRD.

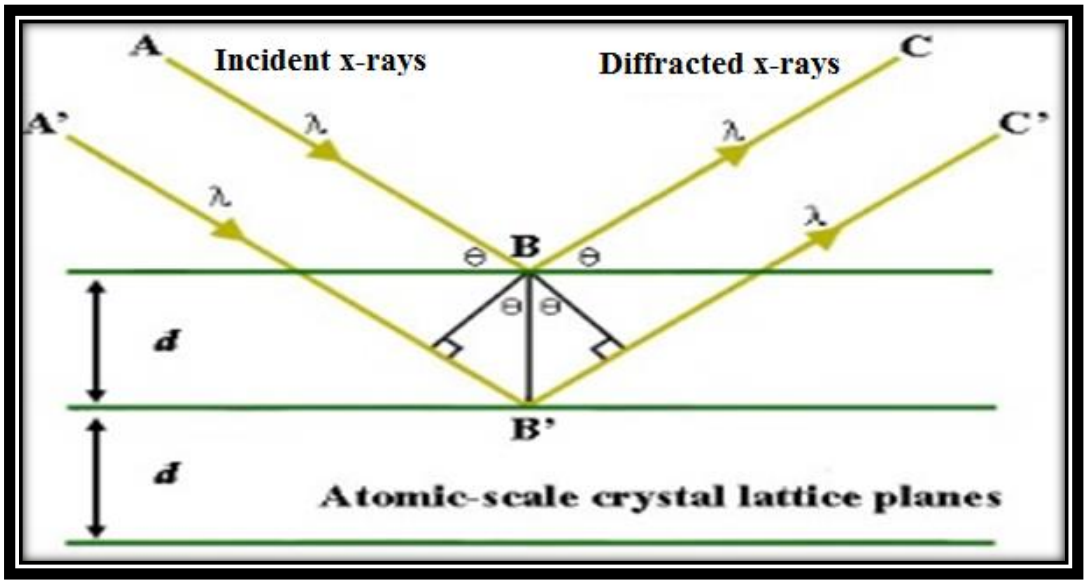

Figure 3.4: Typical principle of XRD through Bragg's law [14].

3.3.2 X-ray Photoelectron Spectroscopy (XPS)

X-ray photoelectron spectroscopy, also known as Electron Spectroscopy for Chemical Analysis (ESCA) is based on the study of the energy distribution of the electrons emitted from compounds irradiated by X-rays; this provides chemical information at the surfaces of compounds of interest. However, in principle, all electrons, from the core to the valence levels, can be investigated using this technique [16]. The basic principle of XPS process involves the ejection of photoelectron from the K level resulting from the interaction of an X-ray photon with a sample as shown schematically in **Figure 3.5**. The energy of the photo-emitted electrons is characteristic of the chemical state of the elements and compounds present i.e. this technique is analytically useful in distinguishing bound-state or multivalent states of individual elements [16, 17]. In this study, a Perkin Elmer Phi 5600 ESCA system from the University of South Africa (UNISA) has been used for XPS analysis to collect and analyze ejected photoelectrons to produce a spectrum of emission intensity versus electron binding energy.

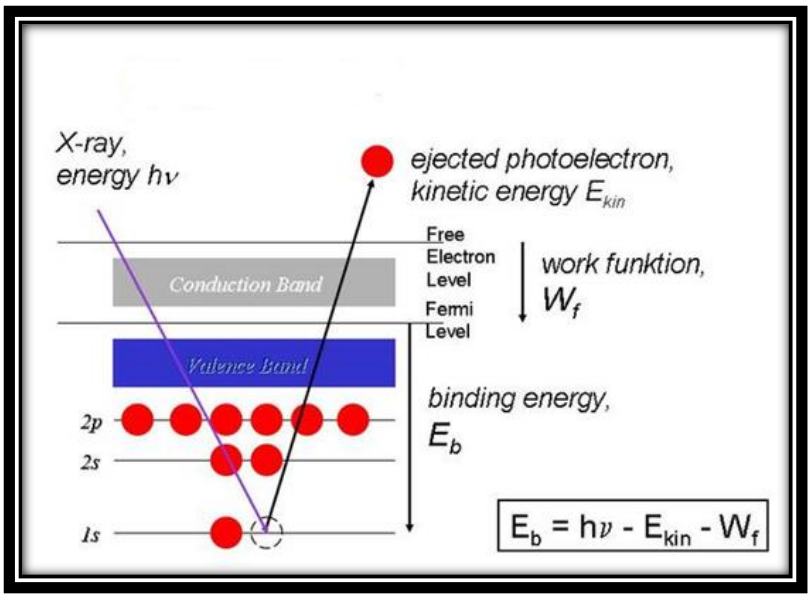

Figure 3.5: Schematic of the photoemission process [16].

3.3.3 Fourier Transform Infrared Spectroscopy (FTIR)

Fourier transform infrared (FT-IR) spectroscopy is the study of interactions between matter and photons in the infrared region. In this region, electromagnetic waves usually excite molecules into the higher vibrational state [18]. The basic principle of FT-IR process can be summarized by the following steps, see **Figure 3.6**.

- A sample is irradiated with an IR radiation
- IR radiation of incident EM wave is either absorbed or transmitted by the sample
- The resulting spectrum represents the molecular absorption and transmission, creating a unique molecular fingerprint of the sample i.e. no two unique molecular structures can produce the same IR spectrum [19]

In this study, FT-IR spectra were taken using a Frontier NIR + SP10 STD (Perkin-Elmer) instrument from the University of South Africa (UNISA).

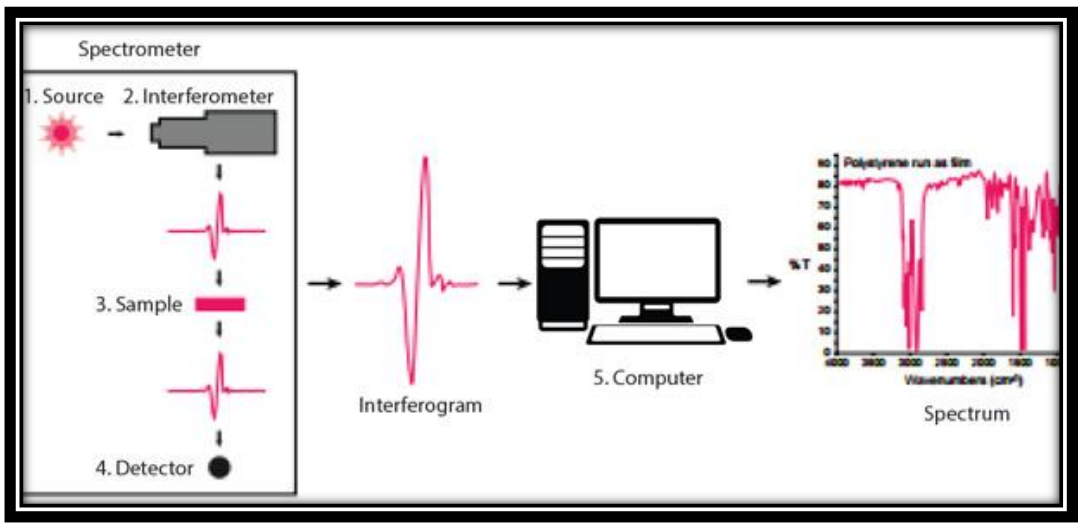

Figure 3.6: Schematic of a typical FT-IR process sample analysis [19].

3.3.4 Scanning Electron Microscopy (SEM)

Scanning electron microscopy (SEM) is a technique whereby highly focused beam of high-energy electrons interacts with a sample to produce various signals that contain information about topography, morphology and crystallography of the sample [20]. Mostly data is collected over a selected area of the surface of the sample, and a 2-D image that displays spatial variations in these properties is generated [21].

The system can also provide qualitative chemical analysis if it is equipped with a dispersive X-ray spectrometer (EDS) [22]. In a typical SEM system, a beam of accelerated electrons with significant amounts of kinetic energy strikes the surface of the sample and generates a splash of electrons with kinetic energies much lower than primary incident electrons called secondary electrons (that produce SEM images). To create a SEM image, the secondary electron intensity is measured as a function of the primary beam position [21].

The advantages of SEM (in contrast to traditional microscopes) include features such as higher magnification (> 100, 000X) and greater depth of field up to 100 times than that of traditional microscope [23]. In this study, SEM images of the specimen were obtained from the JEOL JSM-7500F field-emission scanning microscope (FE-SEM) equipped with energy dispersive X-ray spectrometer (EDX) from the CSIR-NCNSM. **Figure 3.7** shows a simplified layout of SEM.

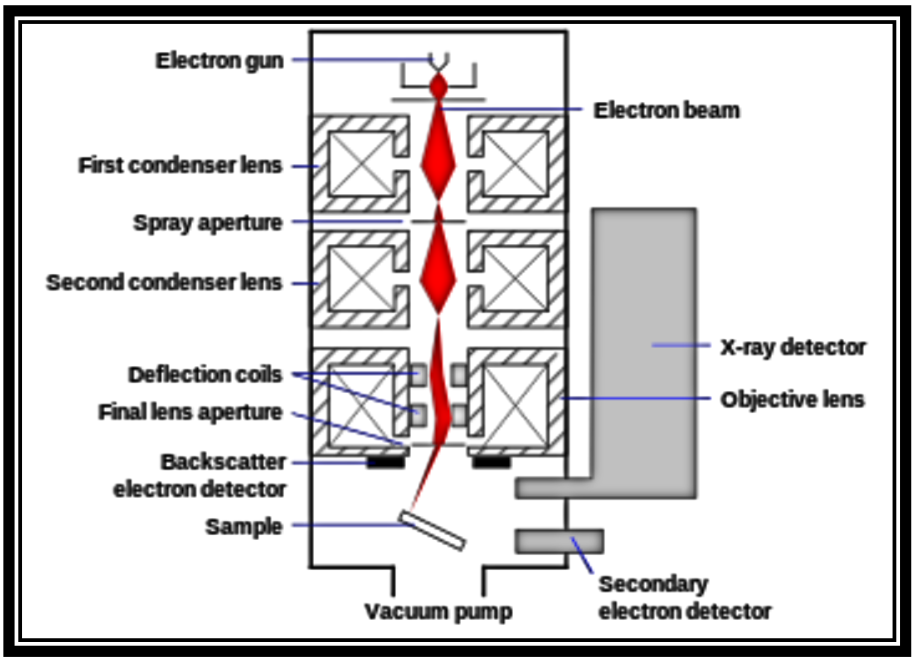

Figure 3.7: A simplified layout of SEM [24].

3.3.5 Transmission Electron Microscopy (TEM)

Transmission electron microscopy (TEM) is an imaging technique in which an interaction between a beam of electrons and ultra-thin specimen generates an image. The resulting image is then magnified and focused onto an imaging device, allowing a detailed quantitative analysis of different materials down to near atomic levels. This kind of analysis is crucial for characterizing materials at a length scale from atoms to hundreds of nanometers.

This technique can be utilized to investigate in fine detail the size, shape, crystallinity, and inter-particle interaction of the specimen [25, 26]. Elemental identification through measurements of characteristic X-ray energies can be done with this technique if it's equipped with EDX [27]. The system is also capable of generating diffraction patterns of the crystalline structures by adjusting its magnetic lenses. Images produced from single crystals can provide information about the space group symmetries in the crystal and the orientation of the planes of atoms in a crystal relative to the electron beam, indicating the dependence of the diffraction pattern on the orientation and the structure of the specimen illuminated by the electron beam [25]. In this study, the TEM images of the specimen were obtained using JEOL-Jem 2100 high-resolution transmission electron microscope (HR-TEM) from the CSIR-NCNSM. A schematic diagram of a TEM system is shown in **Figure 3.8**.

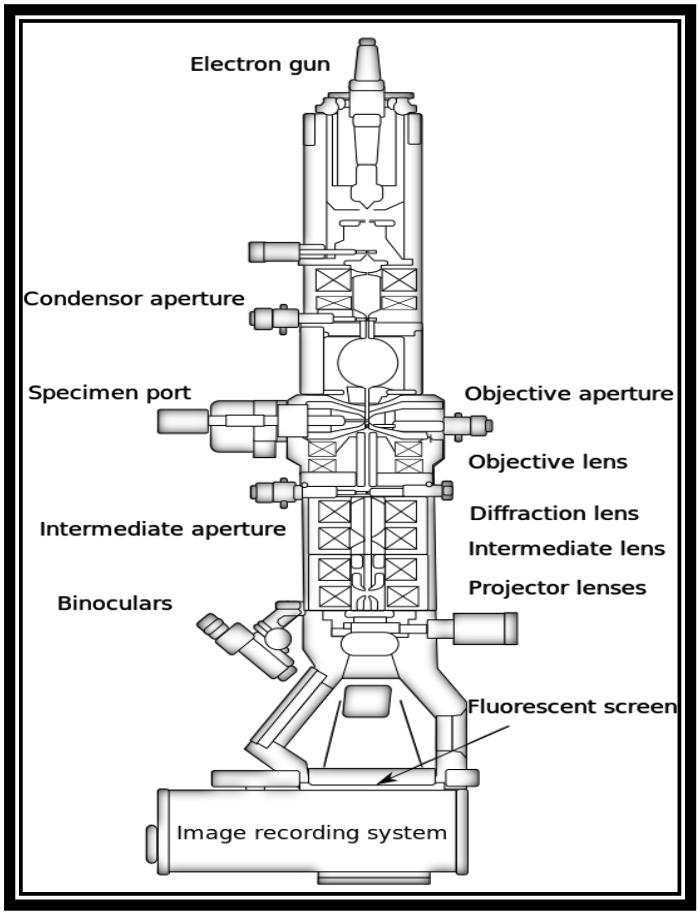

Figure 3.8: A schematic diagram of a TEM system [25].

3.3.6 Ultraviolet/Visible/Near-Infrared UV/Vis/NIR Spectroscopy

The UV/Vis/NIR spectroscopy equipped with an integrating sphere is one of the most important analytical instruments in the modern day laboratory [28]. Integrating sphere (IS) is an optical component consisting of a very highly reflecting inner surface in close proximity to the sample, such that the reflected light enters the sphere wall and finally impinges upon the detector [29]. Using the IS system, the total transmittance and reflectance for samples can be determined by shining light source through the sample from which we can extract the optical properties of the sample in question [29]. In principle, when light interacts with the sample, the light may be absorbed or scattered, transmitted through or diffuse transmitted and reflected straight back or diffusively reflected in various proportions depending on the optical properties of the sample [30]. Therefore, it is crucial to determine absolute values of the sample optical properties for various wavelengths [30]. The actual transmittance is determined by:

$$\boldsymbol{T = It/Io \; or \; \%T = It/Io \; x \; 100} \qquad \textbf{(3.3)}$$

Where I_o, is the intensity of incident light beam when interacting with solely the reflecting surface in the absence of the sample. Whereas I_t is the intensity of the light beam after it passes through the sample [31]. In practice, it is found that UV/Vis/NIR spectrum of most molecules consists of a few humps rather than sharp lines, indicating that the molecule is absorbing/reflecting/transmitting radiation over a band of wavelengths [28]. In this study Lambda 1050 UV/Vis/NIR spectrophotometer (Perkin Elmer) equipped with integrating sphere from UNISA was employed to measure the diffuse reflectance of the samples. **Figure 3.9** shows a typical integrating sphere setup.

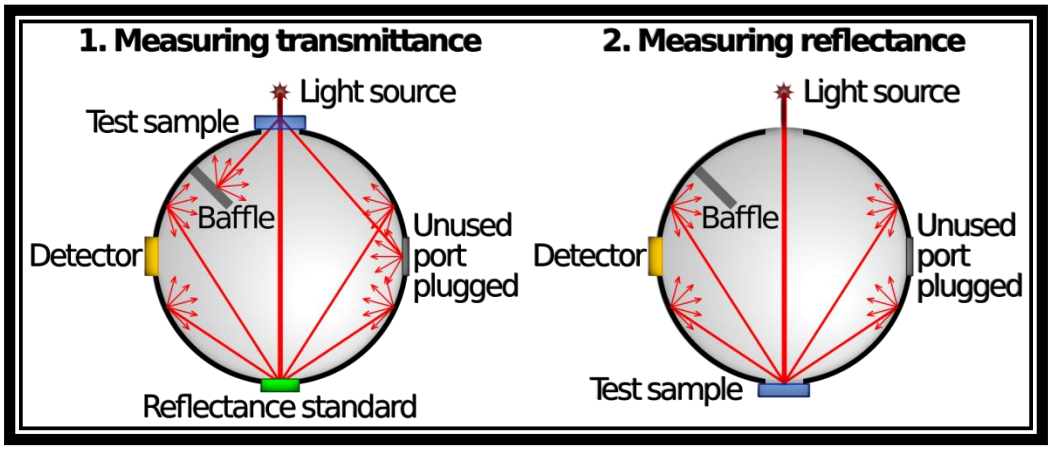

Figure 3.9: Typical Integrating set-up for measuring reflectance and transmittance [32].

3.3.7 Photoluminescence (PL) Spectroscopy

Photoluminescence PL spectroscopy is a non-contact, nondestructive method of probing the electronic structure of materials [33]. In essence, PL can be defined as a process in which an electron is elevated to higher energy upon photon absorption in a process called photo-excitation. After excitation, the electron can return to its equilibrium state via two possible paths; radiative decay (emission of light) and non-radiative decay (emission of phonons). These two are competing processes [34]. The PL process is generally classified in terms of the nature of the electronic transitions generating it [34]. The energy of the emitted light relates to the difference in energy levels between the two electron states involved in the transition between the excited state and the equilibrium state [35]. Optimized PL spectrometers can provide a variety of important properties of light emitting materials such as band gap, impurity levels and defects and material quality [33]. In this study, Fluorolog 3 spectrophotometer from UNISA was employed for photoluminescence measurements. **Figure 3.10** shows a typical schematic experiment of PL system.

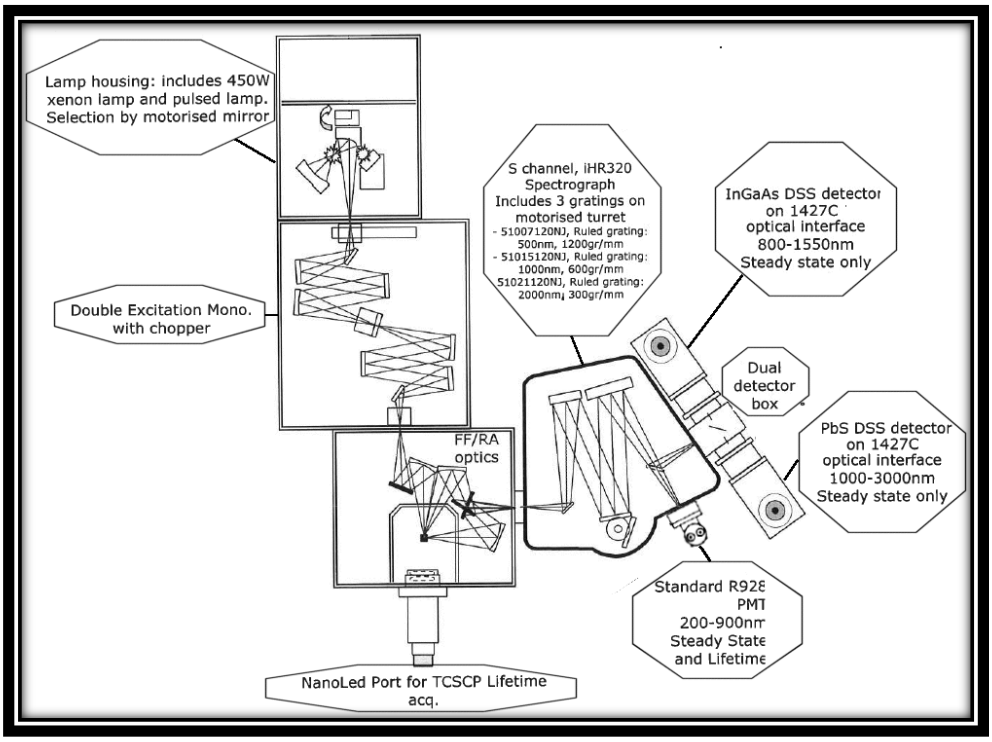

Figure 3.10: System configuration of the PL technique (Fluorolog 3) [36].

Near-Infrared (NIR) spectrometer using a continuous or pulsed beam has emerged as a valuable analytical technique in the field of nanomaterials [37]. This system is available either as a stand-alone device or as an upgrade to a standard PL UV/Vis steady state system [37]. In essence, a laser beam of NIR radiation (low energy radiation) interacts with a sample, and then the sample emits detectable photons of higher energy in the UV/Vis/NIR range in a process called upconversion [38]. Using laser beam as a light source is advantageous (in contrast to LEDs) because laser diodes emit monochromatic radiation and their output is easily focused and manipulated due to coherent nature of the laser beam. The laser beam is very useful for many applications in physics, chemistry, the medical industry, and industrial applications [39]. In this study, a continuous laser beam of 980 nm was used to excite the samples at room temperature using Fluorolog spectrometer (Jobin Yvon) from UNISA.

3.4 References

[1] Choy K.L, *Prog. Mater. Sci*., **2003**, 48, 57-170.

[2] Shimakawa H, Sakamoto F, Tsuchida Y, *Ceram. Powder Sci*., **1993**, 4, 115.

[3] Carp O, Huisman C.L, Reller A, *Prog. Solid State Chem*., **2014**, 32, 33.

[4] Tang Z.L, Zhang J.Y, Cheng Z, Zhang Z.T, *Mater. Chem. Phys*., **2002**, 77, 314.

[5] Klein L.C, Ann. Rev. Mater. Sci., 1985, 15, 227.

[6] Danks A.E, Hall S.R, Schnepp Z, Mater. Horiz., 2016, 3, 91-112.

[7] Yu J.C, Yu J.G, Zhang L.Z, Ho W.K, J. Photochem. Photobiol. A: Chem., 2002, 148, 263.

[8] Criston S, Armelao L, Tondello E, Traldi P, J. Mass Spectrom., 1999, 34, 1380.

[9] http://www.chemat.com/chemattechnology/SolGel.aspx [Accessed 06/02/2017].

[10] https://en.wikipedia.org/wiki/Titanium_isopropoxide [Accessed 19/10/2016].

[11] Chandrakala V, Steffy J.A.J, Praveen B, Pugazhendhi K, Tenkyong T, Jeyarani W.J, Shyla J.M, *Int. J. Tech. Res. App.* **2016**, 37, 16-19.

[12] Chiba H, Tada K, Yamamoto T, Iwanga K, Maniwa A, Yotsuya T, Oshima N, Funakubo H, *TOSOH. Res. & Tech. Rev.* **2011**, 55, 3-6.

[13] Gao G, *Nanostructures, and Nanomaterials: Synthesis, Properties & Applications*, 6th edition, London, **2004**.

[14] Eby G.N, *Principles of Environmental Geochemistry*: Brooks/Cole –Thomson learning, **2004**, 212-214.

[15] Suryanarayana C, Norton M.G, *X-ray diffraction: A Practical Approach*. Plenum Press: New York, **1998**.

[16] Hollander J.M, Jolly W.L, *Acc. Chem. Res.* **1970**, 3(16), 193-200.

[17] www.chem.qmul.ac.uk/surfaces/scc/scat5_3.htm [Accessed 20/10/2016].

[18] www.physics.nus.edu.sg/~L3000/Level3manuals/FTIR.pdf [Accessed 20/10/2016].

[19] https://cma.tcd.ie/misc/ftir.pdf [Accessed 20/10/2016].

[20] http://www.unl_edu/CMRACfem/semoptic.htm. [Accessed 20/10/2016].

[21] http://serc.carleton.edu/research_education/geochemsheets/techniques/SEM.html. [Accessed 20/10/2016].

[22] http://nue.clt.binghamton.edu.semtem.html [Accessed 23/10/2016].

[23] Garcia Sole J, Bausa L.E, Jaque D, *An Introduction to the Optical Spectroscopy of Inorganic Solids*, John Wiley & sons Ltd (**2005**).

[24] https://en.wikipedia.org/wiki/Scanning_electron_microscope [Accessed 20/10/2016].

[25] https://en.wikipedia.org/wiki/Transmission_electron_microscopy [Accessed 20/10/2016].

[26] Wang Z.L, Liu Y, Zhang Z, *Handbook of nanophase and nanostructured materials*, 4th Ed, New York, **2003**.

[27] https://www.oxford-instruments.com [Accessed 22/10/16].

[28] http://www.uni-salzburg.at/fileadmin/oracle_file_imports/359201.PDF [Accessed 24/10/16].

[29] Integrating Sphere Theory
http://www.chemistry.adelaide.edu.au/external/soc-rel/content/beerslaw.htm
[Accessed 15/06/2016].

[30] A guide to Integrating Sphere Theory and Applications
http://www.labsphere.com/data [Accessed 17/11/2009].

[31] http://www.shimadzu.com/an/uv/support/fundamentals/structure.html [Accessed 24/10/16].

[32] https://en.wikipedia.org/wiki/Integrating_sphere [Accessed 24/10/16].

[33] http://www.horiba.com/scientific/products/photoluminescence/ [Accessed 25/10/16].

[34] Mhlongo G.H, *Luminescence investigation of trivalent rare earth ions in sol-gel derived $SiO_2$and ZnO co-doped SiO_2: Pr^{3+}*, [Ph.D. Thesis], **2011**, University of the Free State, South Africa.

[35] Peter Y. Yu and Manuel Cardona, *Fundamentals of Semiconductors: Physics and Materials Properties*, Springer Heidelberg Dordrecht London New York, **(2010).**

[36] Kabongo G.L, *Luminescence investigation of zinc oxide nanoparticles doped with rare earth ions*, [MSc. Thesis], **2013**, University of South Africa, South Africa.

[37] www.pti-nj.com/brochures/QuantaMaster.pdf [25/10/16].

[38] Chatterjie D.K, Gnanasammandhan M.K, Zhang Y, *Small*, **2010**, 6(24), 2781-2795.

[39] http://www.ophiropt.com/user_files/laser/beam_profilers/C_Roundy_Tutorial.pdf [Accessed 25/10/2016].

Chapter 4: Sol-gel Synthesis and Characterization Studies of Er^{3+} Doped TiO_2 Nanoparticles

In the current chapter, down-and up-conversion luminescence behaviour of sol-gel derived erbium doped titanium dioxide with anatase structure. Through combined structural, optical and electron microscope analysis, effective and influence of Er^{3+} doping into TiO_2 lattice has been demonstrated using X-Ray diffraction (XRD), scanning electron microscope (SEM), transmission electron microscope (TEM), and optical reflectance spectra. XRD results showed only anatase diffraction peaks of TiO_2, indicating the formation of a pure anatase phase even after Er^{3+} incorporation into TiO_2 lattice. Selected Area Electron Diffraction (SAED) confirmed that the synthesis of TiO_2 nanoparticles are polycrystalline in nature which correlated well with XRD findings. Upon excitation at 320 nm, two down-conversion contributions at 378 nm and 435 nm attributed to indirect band gap and defect-related emissions, respectively were observed from both pure and Er^{3+} doped TiO_2 nanoparticles. On the other hand, strong green up-conversion emission centered at 544 nm ascribed to $^4S_{3/2} \rightarrow {}^4I_{15/2}$ transition of Er^{3+} was observed under 980 nm laser excitation for all Er^{3+} doped TiO_2 samples. This result analysis brings insight on understanding of structural, optical and luminescence properties of Er^{3+} doped TiO_2 nanoparticles for use in solar cells.

4.1 Introduction

For many years, extensive research activities have been focused on materials displaying low energy photon emissions obtained by exciting the material with high-energy photons, through a process referred to as down-conversion. However in recent years, due to the rapid development of nanotechnology; several investigations of host materials doped with up-converting rare-earth (RE) ions have been carried out due to their photoluminescent properties [1, 2]. Up-conversion is an optical process whereby a photon of higher energy is emitted by a phosphor following an excitation by two or more low energy photons [1, 3, 4]. The process is known to occur when a suitable rare-earth ion is doped in fluorides, oxysulfides, and oxides [5, 6]. This makes it mandatory to carefully select a good combination of the host lattice and dopant ions in order to improve the efficiency of the up-conversion process [3, 7]. These remarkable luminescence properties make such materials suitable candidates to use in solar cells [8], lasers [9], sensors, and bio-optical imaging [3].

In this study, anatase TiO_2 was selected as the host lattice due to its relatively low phonon energy (639 cm^{-1}) [10]. High phonon frequencies of the host lattice lead to non-radiative relaxation, consequently resulting in weaker up-conversion luminescence [11]. Other contributing factors towards the selection of TiO_2 as a host are; high refractive index of 2 [12], low cost and non-toxicity [13], high photochemical stability [14] and suitable energy band structure [15]. However, effective applications of TiO_2 are limited due to its wide band gap (3.2 eV) which only allows TiO_2 to absorb ultraviolet (UV) light, which only accounts for about 4% of the solar electromagnetic spectrum [16]. In order to overcome this drawback, the following were attempted in order to modify the optical properties of TiO_2; addition of transition metal ions [17], sensitizing TiO_2 using dyes [18] and doping with up-conversion luminescence agents [19].

The latter approach proved effective in improving the visible optical properties of TiO_2 in order to broaden its applications [2, 3]. Among many rare-earth ions, only a few (e.g. Er^{3+} and Tm^{3+}) ions have been recognized as the most efficient up-converting materials [1]. Er^{3+} ion is considered as one of the most suitable elements for improving up-conversion efficiency in various host materials due to its long-lived excited states [6]. One of the most attractive attributes of Er^{3+} in the up-conversion process is the location of the energy levels $^4I_{13/2}$, $^4I_{9/2}$, $^2H_{11/2}$ /$^4S_{3/2}$ and $^2H_{9/2}$, which are nearly equidistant, and therefore match the excitation wavelength of the ground state [20]. When incorporated in a solid host, Er^{3+} ions show well-defined energy levels of the 4f-shell electronic configurations [21]. Different up-conversion luminescence mechanisms can take place either alone or in a combination, but one process is usually more dominant than others [22]. Up-conversion has two basic predominant mechanisms; energy transfer up-conversion (ETU) and excited-state absorption (ESA) [19], with ETU having the highest probability and it is far more efficient up-conversion process than ESA [23].

The development of facile synthetic methodologies for Er^{3+} doped TiO_2 novel luminescent nanoparticles with controlled and uniform crystalline phase, shape and size is very crucial to manipulating their optical properties and exploring their potential applications in diverse fields. For this reason, various chemical approaches including sol-gel [24], chemical vapour decomposition (CVD) [25], and microwave assisted method [26] to mention a few have been developed. Among them, this study has been devoted to the sol-gel method due to its unique features such as ease of synthesis [27], synthesis of high purity nano-sized crystalline powders at low temperatures [28] and better homogeneity and production of high purity powder [29]. TiO_2 doped with an intention of producing up-converted luminescence has not been fully explored. In this study, we demonstrate the effective and effect of Er^{3+} varying concentration on both down-conversion and up-conversion luminescence in TiO_2 host. Structural, morphological, molecular functional groups as well as optical absorption analysis through various techniques have been done.

4.2 Experimental detail

4.2.1 Synthesis of pure and Er^{3+} doped TiO_2

The chemical reagents used in the current experiments were analytical grade and were used as purchased from Sigma-Aldrich, South Africa. Pure TiO_2 nanopowders were prepared by homogeneous hydrolysis of titanium isopropoxide (TTIP, 99%) aqueous solutions using Isopropyl alcohol (70% in H_2O) as the precipitation agent. In a typical experimental procedure, 15 ml of TTIP was added dropwise in 100ml of isopropyl alcohol and agitated at room temperature for 10 mins. Then 10ml of de-ionised water was added to the above mixture and was hydrolyzed for 2 h at room temperature under vigorous magnetic stirring. For preparation of Er^{3+} doped TiO_2 with various Er^{3+} doping concentrations, stoichiometric amounts of $Er(NO_3)_3 \cdot 5H_2O$ (99%, Sigma-Aldrich) corresponding to 1, 3, and 8 mol% doping levels were fully dissolved in the TTIP in isopropanol/de-ionised water mixture. The resultant solutions were then aged for 24 h at room temperature to form the derived gels which were harvested by centrifugation, washed and dried at 80 °C in an electric oven for 24 h for the removal of excess organics and water. To produce pure and Er^{3+} doped TiO_2 nanopowders, the as-prepared samples were calcined at 400 °C for 2 hours in a muffle furnace.

4.2.2 Characterization

X-ray diffraction (XRD) powder patterns of the synthesized samples were recorded by Smartlab X-ray diffractometer (Rigaku) equipped with CuKα (λ = 1.5406 Å) X-ray source. The analysis pertaining the crystallinity, size and shape of samples were carried out on an Auriga Cobra FIB field emission scanning electron microscope (FE-SEM) coupled with energy dispersive X-ray spectroscopy (EDS) which was used to conduct elemental analysis and JEOL 2100 High-resolution

transmission electron microscopy (HRTEM) operated at 200kV. The reflectance characteristics of the powders were determined using the 1050 UV-Vis-NIR absorption spectrophotometer (Perkin Elmer) equipped with an integrating sphere. The functional groups of the samples were studied by a Spotlight 400 FTIR imaging system using the diffuse reflectance mode from 550 to 4000 cm^{-1}. Photoluminescence data including emission spectra and up-conversion measurements of all the synthesized samples were recorded on a Horiba, Jobin Yvon Fluorolog 3 Photoluminescence spectroscopy under excitation of a Xenon lamp and a continuous LED laser beam of 980 nm wavelength, respectively.

4.3 Results and Discussion

4.3.1 Influence of Er doping on Structural properties.

The XRD patterns of pure and Er^{3+} doped TiO_2 nanoparticles with different concentrations of Er ions are shown in **Figure 4.1**. As observed from Figure 2, the structure of the synthesized pure and Er^{3+} doped TiO2 samples has been identified as anatase crystalline phase of TiO_2 according to the standard JCPDS no. 86-1157 [30]. No additional peaks corresponding to any polymorph of neither TiO_2 nor impurities were observed in the XRD patterns, indicating that Er^{3+} was successfully incorporated as a dopant. The intensity of the diffraction peaks declined significantly with increasing Er^{3+} concentration which is indicative of the reduction in the crystallinity of the samples with Er addition probably due to the disorder caused by the substitution of Er^{3+} ions (0.0881 ionic radii) into the sites of Ti^{4+} ion (0.0605 nm ionic radii) [31, 32]. This is manifested by a very small shift slightly towards higher 2θ angles for the main (101) peak with incorporation of Er^{3+} into TiO_2 lattice (see insert in **Figure 4.1)** which can be attributed to lattice mismatch, distortion, and crystal strain [33].

The diffraction peak shift in this regard can therefore be regarded as indirect evidence of successful Er^{3+} doping into the TiO_2 lattice. Furthermore, the broadening of the diffraction peaks with Er^{3+} increasing concentration in this case confirms the reduction in the grain size with Er^{3+} addition. To confirm this observation, the crystallite sizes of all the samples were calculated from the full width at half maximum (FWHM) of the most intense (101) anatase peak using the well-known Scherrer formula [33]. For pure TiO_2, the crystallite size was found to be 8.3 nm which decreased to 7.8, 6.5 and 6.7 nm for 1, 3, and 8 mol% Er, respectively, implying that the introduction of Er^{3+} ions into TiO_2 lattice may hinder the growth of the crystallite due to the segregation of the dopant cations at the grain boundary [34].

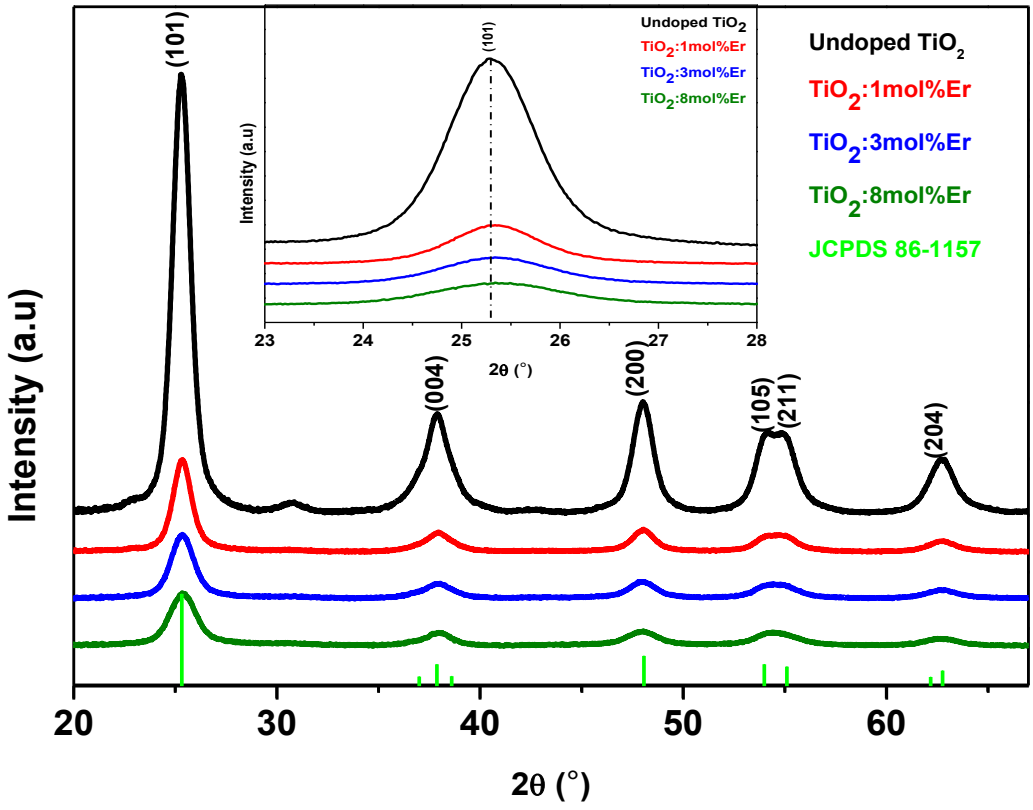

Figure 4.1: The XRD patterns of pure and Er^{3+} doped TiO_2 nanoparticles with different Er concentrations as well as the standard. The insert shows the magnified region of (101) peak.

For structural and microstructural examination of pure and Er^{3+} doped TiO_2 nanoparticles, SEM and TEM analyses were performed. **Figure 4.2 (a)** and **(c)** show the SEM images of the synthesised TiO_2 products prior and after Er^{3+} doping with different concentrations. In this case, 8 mol% doped TiO_2 sample was selected for both SEM and TEM examinations. For pure TiO_2, sample, it was realized that the particles crystallized into irregular shapes, and are agglomerated. The particle-like features was still maintained even after addition of various concentrations of Er^{3+} ions into TiO_2 (see **Figure 4.2 (b)**). To further confirm the presence and distribution of Er, Ti, and O elements, EDS elemental maps were collected (see **Figure 4.2 (c-d)**). For both pure TiO_2 and Er doped TiO_2 samples, the corresponding elemental maps of Ti (**Figure 4.2 (e)**) and O (**Figure 4.2 (f)**), and Ti (**Figure 4.2 (g)**) and O (**Figure 4.2 (h)**), and Er (**Figure 4.2 (i)**) elements were extracted.

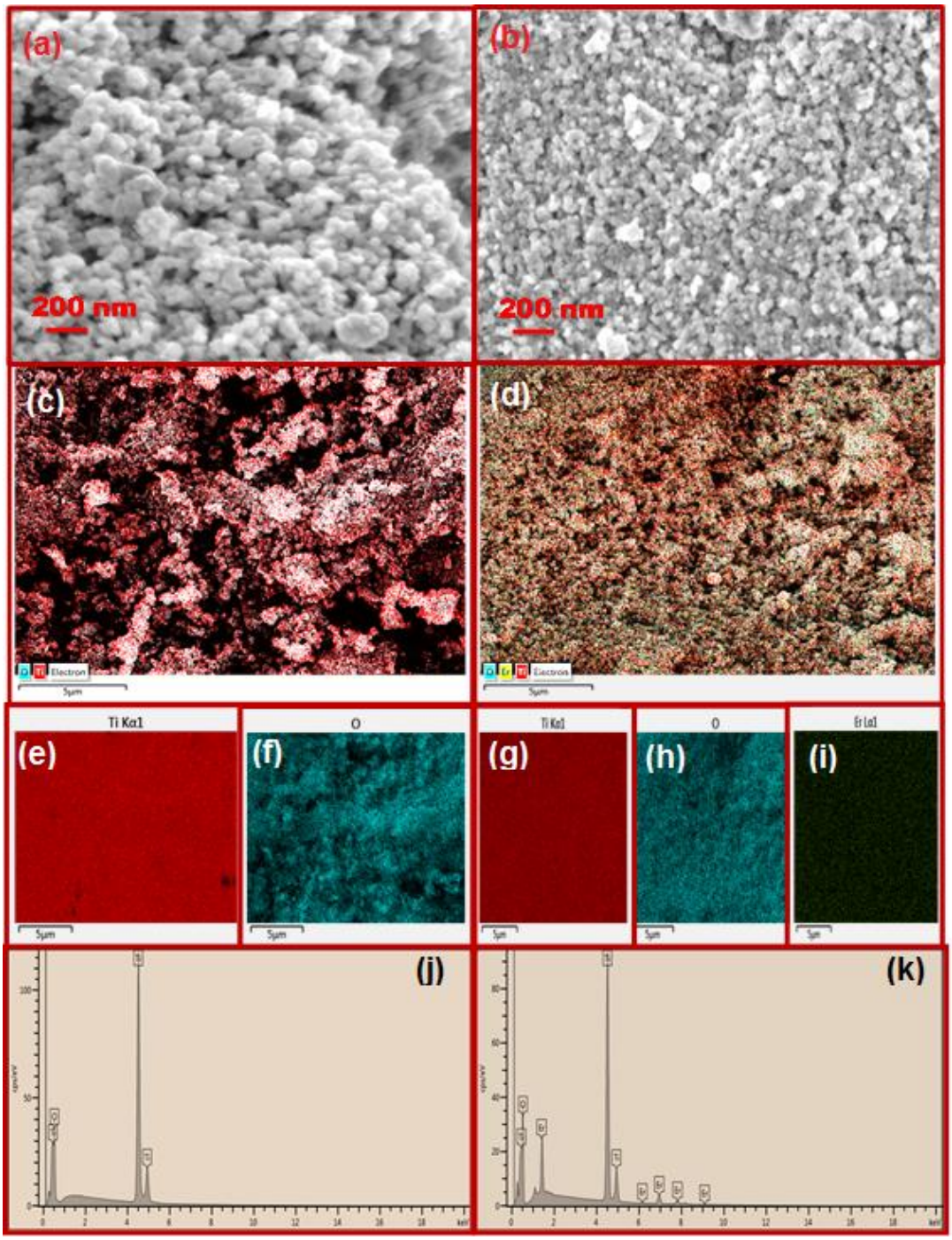

Figure 4.2: **(a, b)** SEM micrographs, **(c-i)** elemental maps, and **(j-k)** EDS spectra of pure and Er^{3+} doped TiO_2 nanoparticles.

These elemental maps revealed uniform distribution of Ti, O, and Er elements. The EDS spectra shown in **Figure 4.2 (j)** and **(k)** further confirmed the presence of erbium in the doped sample. **Figure 4.3 (a)** and **(c)** shows TEM micrographs of pure and Er^{3+} doped TiO_2 nanoparticles. The micrographs obtained from both pure and Er^{3+} doped TiO_2 showed agglomerates of nanosized TiO_2 particles, which is in accordance with SEM findings. High resolution TEM observations were collected to further understand structural properties of the samples and are shown in **Figure 4.3 (b and d)**. A closer analysis of the HRTEM observations (see **Figure 4.3 (b and d)**) revealed clear fringes with inter-planner spacing of ~0.54 nm corresponding to the (1 0 1) lattice planes of anatase TiO_2 for both pure and Er^{3+} doped TiO_2 samples which correlates with the XRD results. Additional structural characterization through selected area electron diffraction (SAED) patterns (see inset in **Figure 4.3 (b and d)**) displayed spherical rings in electron diffraction patterns which indicates that the synthesized TiO_2 nanoparticles are polycrystalline in nature. The histograms presented in **Figure 4.3 (e)** and **(f)** shows the grain size distribution in pure and Er^{3+} doped TiO_2 samples where the decrease in average particle size with Er^{3+} addition from 7.8 nm in diameter for pure TiO_2 to 6.7 nm for 8 mol% Er^{3+} doped TiO_2 was observed. This observation agrees well with XRD results. The decreasing trend in grain size in this case could be to the fact that when more and more Er^{3+} ions are doped into TiO_2 lattices, the distortion of the TiO_2 lattice structure occurs and this results in formation of internal strain which then hinders grain growth. These results indicate the particle size of the Er^{3+} doped TiO_2 samples can be tuned to some extent by controlling the dopant concentration [35].

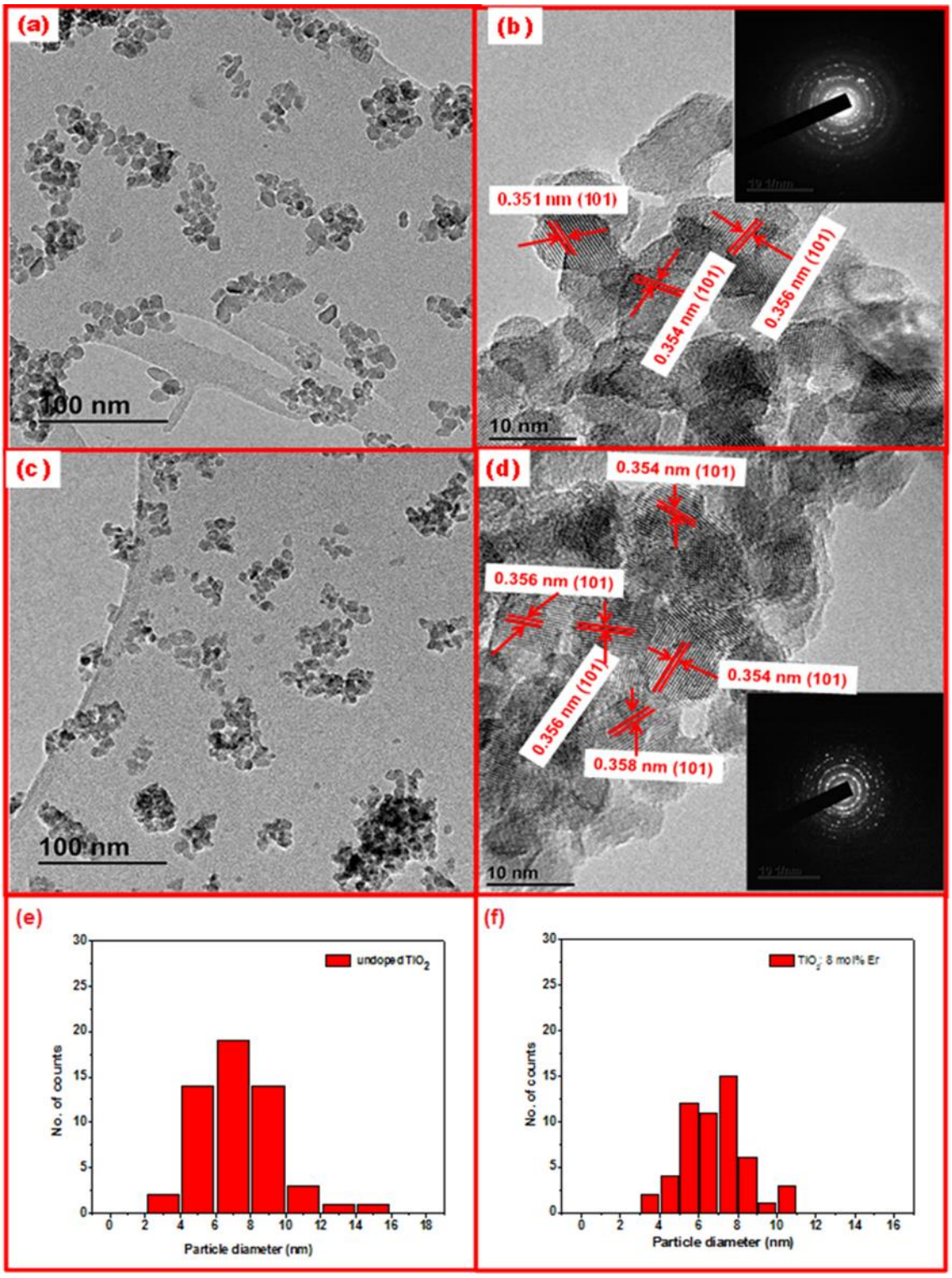

Figure 4.3: TEM images of **(a)** undoped TiO_2, **(c)** 8mol% Er^{3+} doped nanopowders. HRTEM images of **(b)** undoped TiO_2 and **(d)** 8mol% Er^{3+} doped nanopowders and particle size distribution of **(e)** undoped TiO_2, and **(f)** 8 mol% Er^{3+} doped nanopowders.

4.3.2 Optical properties

Figure 4.4 shows FT-IR transmittance spectra of pure and Er^{3+} doped TiO_2 nanoparticles with various Er^{3+} concentrations. It is obvious from this figure that all the FT-IR transmittance spectra are composed of three distinct bands. The bands at higher wavenumbers at 3200 cm^{-1} which can be ascribed to the OH^- vibrations as well as those between 1400 and 1700 cm^{-1} originating from υ[C=C, C=O] and δCH_3 vibrations due to the organic residues. The bands at lower wavenumbers between 650 cm^{-1}/0.08 eV and 850 cm^{-1}/0.1 eV can be assigned to Ti-O-Ti vibration [36]. This energy range is sufficient to account for some of the phonon assisted non-radiative transitions between intermediate states of Er^{3+} with small energy levels separation such as $^2H_{11/2} \rightarrow {}^4S_{3/2}$ and $^4F_{5/2} \rightarrow {}^4F_{3/2}$, indicating that the non-radiative relaxation depends on the separation between the excited level and the level just below it [37]. The intensity of the peaks is reduced with an increase in the dopant concentration, and this corresponds with the disappearance of hydroxyl and organic contaminants.

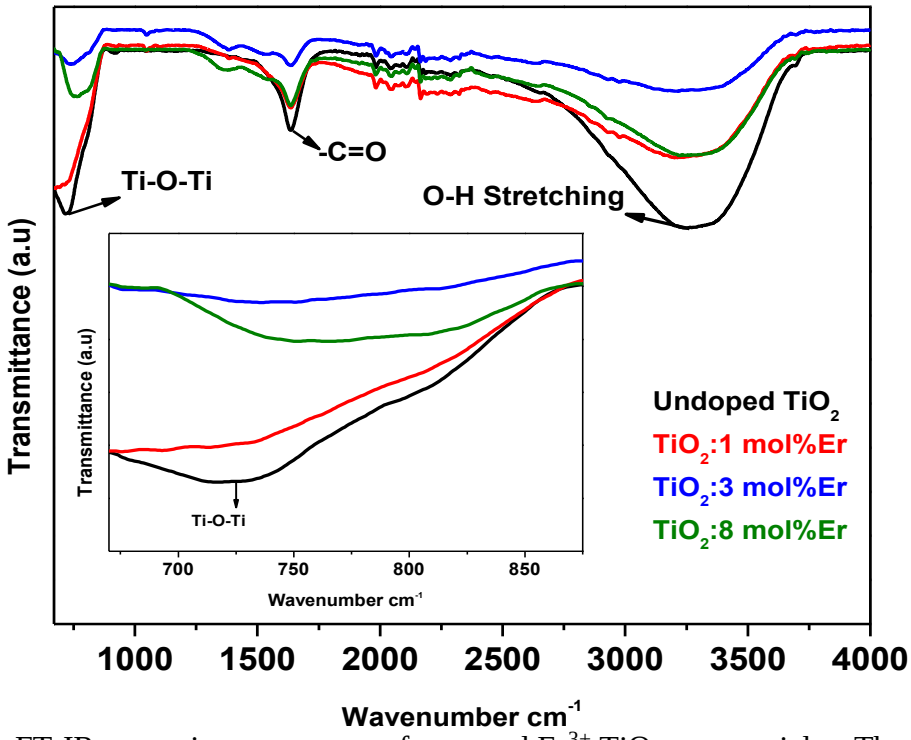

Figure 4.4: FT-IR transmittance spectra of pure and Er^{3+} TiO_2 nanoparticles. The insert shows the magnified region showing Ti–O–Ti vibrations.

To study the optical absorption properties of pure and Er^{3+} doped TiO_2 nanoparticles, diffuse reflectance spectra were examined and are shown in the insert of **Figure 4.5**. The observed sharp band edge at ≈ 350 nm for the pure TiO_2 sample could be due to the intrinsic band gap absorption of TiO_2 [38]. For pure TiO_2, no absorption in the visible light region above 400 nm could be seen, while Er^{3+} doped TiO_2 nanoparticles showed five absorption peaks in the diffuse reflectance curve at ≈ 453, 490, 523, 544, and 654 nm corresponding to the transition of Er^{3+} from ground state $^4I_{15/2}$ to the excited states $^2F_{3/2}$, $^2F_{7/2}$, $^2H_{11/2}$, $^4S_{3/2}$, and $^4F_{9/2}$, respectively. These peaks are in agreement with visible-light absorbability for Er^{3+} doped samples, suggesting the creation of some intermediate energy levels in the band gap that makes them susceptible in the visible region [39].

For both undoped and doped samples, the optical band-gap values were calculated on the basis of optical spectral absorption using the equation $F(R_\infty) = \frac{A(hv-Eg)^n}{hv}$, where $F(R\_\infty) = \frac{(1-R_\infty)^2}{2R_\infty}$, is the Kubelka Munk function [31], R_∞ represent the ratio between the diffuse reflectance from the sample and a reference material. A is a constant while hv is the incident photon energy, n is 1/2 or 2 for indirect and direct transitions, respectively. Therefore, the optical band-gap values of the samples obtained after extrapolating the linear part of the plot of $[F(R_\infty)hv]^2 vs(hv)$ (see **Figure 4.5**) for hv equal to zero were found to be 3.47, 3.32, 3.32, and 3.44 eV for pure, 1, 3, and 8 mol% Er^{3+} doped TiO_2, respectively. It can be seen that the Er^{3+} doped samples showed a slight decrease in the value of optical band gap as compared to the pure TiO_2 sample. This minor decrease in the band gap value with 1 and 3 mol% Er^{3+} addition correlates with the red shift observed in the optical reflectance results indicating band gap narrowing. The band gap narrowing, in this case, occurs when shallow donor impurities create energy levels in the bandgap near the conduction band edge and shallow acceptor impurities create energy levels near the valence band edge, now with the increase in the amount of doping, the density of states of these dopants increase and forms a continuum of states just like in the bands and effectively the band gap decreases [40].

J Yang et al [41] attributed the red shift of the optical absorption edge of TiO_2 with increasing Er^{3+} content to substitution Ti^{4+} ions by Er^{3+} in the TiO_2 lattice with the introduction of defects or impurity levels.

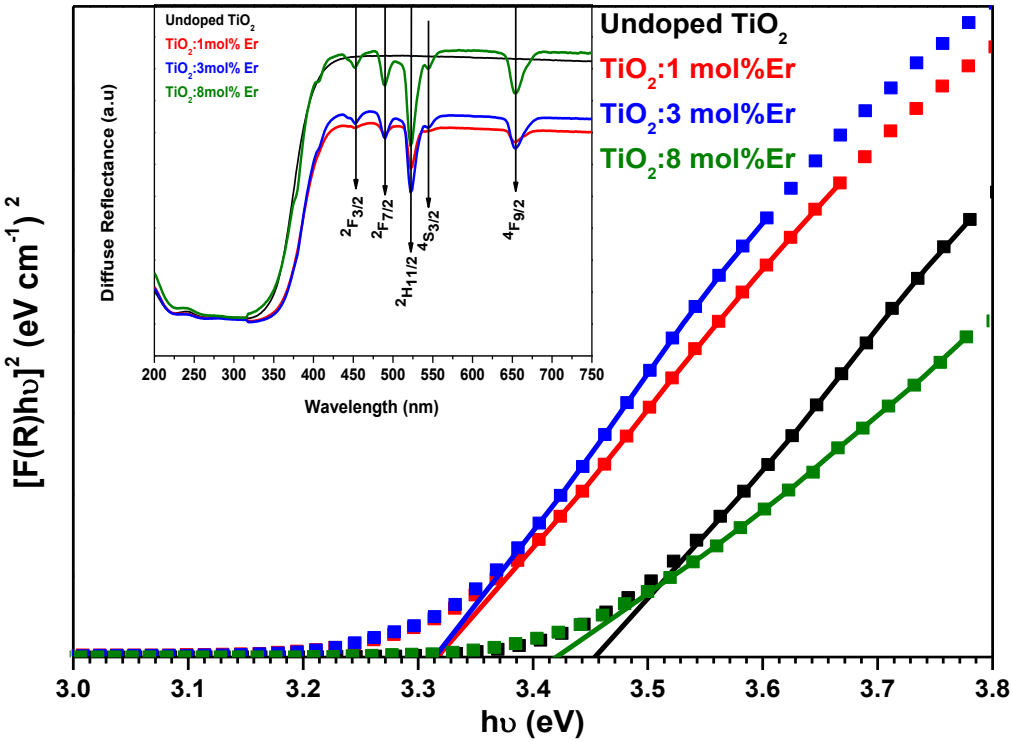

Figure 4.5: UV-Vis-NIR diffuse reflectance spectra of pure, 1, 3, and 8 mol% Er^{3+} doped TiO_2 nanopowders. Kubelka-Munk plot obtained from UV-Vis-NIR spectra are shown as an insert.

4.3.3 Photoluminescence properties

4.3.3.1 Down-conversion

TiO_2 nanoparticles have a high surface area-to-volume ratio, this results in the tremendous influence of surface defects on their performance in photo-catalysis and solar energy conversion [42, 43]. Photoluminescence is a versatile and commonly used tool to investigate the efficiency of charge carrier trapping, immigration and transfer in semiconductors [44].

Additionally, it is more advantageous to use PL spectroscopy in contrast to the traditional photo-absorption spectroscopy due to its superior sensitivity to the surface parameters of nanoparticles [45].

Figure 4.6 shows room temperature PL behaviour of the pure and Er^{3+} doped TiO_2 nanoparticles at an excitation wavelength of 320 nm using Xe lamp. Due to the large band gap of nanophase TiO_2; there are always many active states on TiO_2 surface under continuous UV irradiation [46]. Two emission peaks observed at 378 nm (UV emission), and 435 nm (visible emission) are attributed to indirect band gap and defect-related emissions, respectively [47]. In general, oxygen vacancies can exist in three distinct charge states: the neutral oxygen vacancy, the singly ionized oxygen, and the doubly ionized oxygen vacancy. However, among the three states; many luminescent centers are created solely by the singly ionized oxygen vacancies. When the material is irradiated by UV light, the oxygen vacancies which evolve during the growth of the material trap holes generated by UV exposure. The recombination of the hole with the electron already trapped at the oxygen vacancies emits light which is generally in the visible region [48, 49].

To gain more understanding about the origination of the emission bands in the UV and visible region in the current study, both two contributions were de-convoluted into six sub-peaks using a Gaussian fitting method. In this case the most intense spectrum was selected. The strong UV emission peak at 378 nm is related to phonon-assisted indirect transition from host TiO_2 arising from the edge (X) to the center of (Γ) of Brillouin zone, X_{1b} to Γ_3 [50]. The emission bands located at 385, 418 and 435 nm can be assigned to self-trapped excitons positioned at the TiO_6 octahedron, while those at 449 and 476 nm can be ascribed to shallow trapped oxygen vacancies (Vo) [48, 49, 51]. It is also important to note that there is neither any Er^{3+} emission peak nor there is any significant shift in the position of the defect emission peaks. However, doping with Er^{3+} disturbs

the TiO_2 lattice by breaking the Ti–O bond and generating many oxygen vacancies; these vacancies can either act as luminescence enhancer or quencher [52].

The increase in the emission intensity (visible region) upon doping with Er^{3+} ions can be attributed to the increase of radiative oxygen vacancy centers. It is also observed that the 1 mol% Er^{3+} doping has the most intense UV emission. This can be ascribed to an effective energy transfer from TiO_2 to Er^{3+} ions resulting in the improved photoluminescence (PL) emission. However, at higher concentrations; Er^{3+} ions either tend to locate on a crystal surface, creating undesired Er-Er sites or form Er_2O_3 aggregates, which act as quenching sites, consequently leading to a drastic decrease in the luminescence intensity [53]. The PL emission bands in UV and visible region suggests the application of these materials in various optoelectronic devices and as light emitters in the visible region.

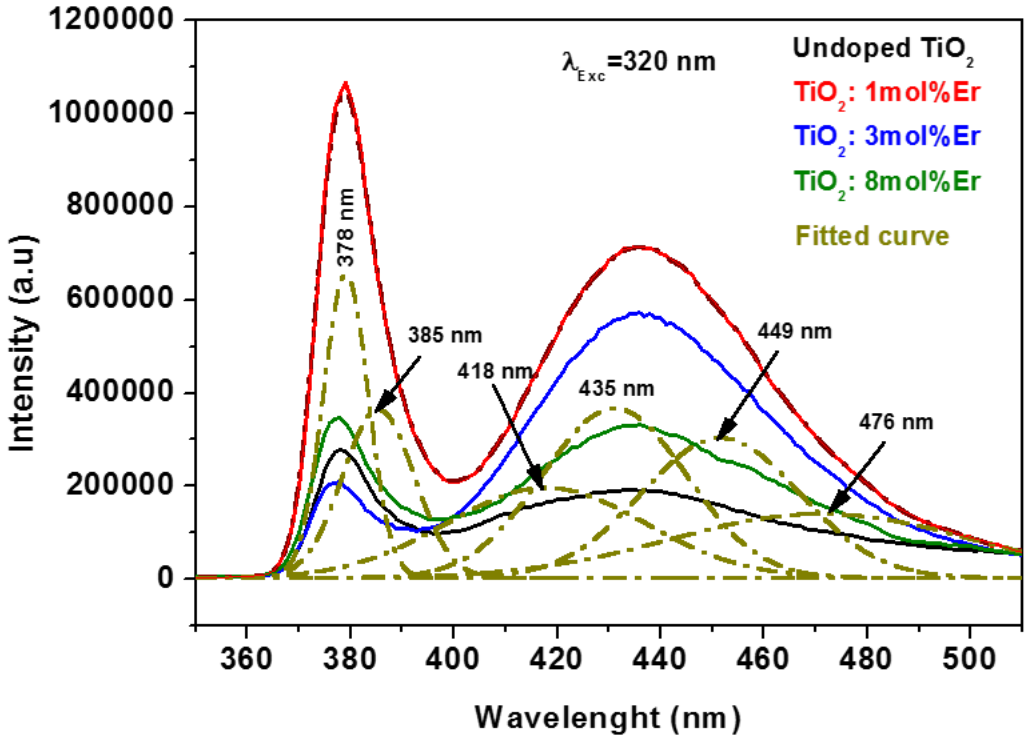

Figure 4.6: PL down conversion emission spectra of as prepared and Er^{3+} doped TiO_2 nanoparticles at an excitation wavelength of 320 nm.

4.3.3.2 Up-conversion studies

Up-conversion processes are ubiquitous among Er^{3+} compounds due to its favourable f-f energy level structure, thus in this section; we report on the up-conversion studies of Er^{3+} doped nanocrystalline TiO_2, as a function of erbium concentration (1, 3, and 8 mol%). The phase of the host lattice is highly influential towards the spectral nature of the up-conversion fluorescence emission [10]. Naturally, TiO_2 exists in two "main" polymorphs, namely; anatase (in which TiO_6 octahedra share faces) and rutile phases in which TiO_6 octahedra share only edges. Therefore, the crystal field is characteristic of a particular crystal phase. Hence the nature of emission arising from two different phases should be unique [19]. **Figure 4.7** shows up-conversion luminescence spectra of the pure and Er^{3+} doped TiO_2 nanopowders (1, 3 and 8 mol%) ranging from 400 to 700 nm, after the samples were excited with a 980 nm laser beam. The emission spectra consist of intense green emission centred at 543 nm corresponding to Er^{3+}: $^4S_{3/2} \rightarrow {}^4I_{15/2}$ transition [6] with the 8 mol% doped TiO_2 sample showing the strongest green emission intensity. This observation strongly indicates that in the TiO_2 nanoparticles, the up-conversion process depends not only on the crystal phase but also on the Er^{3+} concentration. **Figure 4.8** display the schematic energy level diagram of the up-converted emission from Er^{3+} doped TiO_2 sample under infrared excitation. Upon infrared excitation at 980 nm, the electrons will be excited from ground state $^4I_{15/2}$ (GSA) to $^4I_{11/2}$ excited metastable state followed by further excitation to $^4F_{7/2}$ (ESA) level. The excited electrons decay non-radiatively from the $^4F_{7/2}$ level through multi-phonon process to populate both ($^2H_{11/2}$/$^4S_{3/2}$) and $^4F_{9/2}$ excited states, then decay further to ground state ($^4I_{15/2}$) resulting in green and red emission lines generated, respectively. Some of the electrons will decay radiatively from the $^4F_{7/2}$ level to ground state ($^4I_{15/2}$) which resulted in a bluish line emission at 488 nm.

The up-conversion luminescence quenching due to an increase in dopant content is also known as concentration quenching- during this process, Er^{3+}–Er^{3+} dipole-dipole energy transfer is highly dependent on the distance R between interacting ions and according to resonant energy theory, it follows a $1/R^6$ dependence [54]. This dependence shows that at high Er^{3+} concentrations, the separation between Er^{3+} neighbouring ions becomes so close that the energy is transferred among them leading to the creation of quenching centers, consequently resulting in a reduction of the up-conversion luminescence intensity. It is worth mentioning that the NIR light was successfully absorbed and re-emitted in the visible region by the materials produced in this study; these materials have many advantages over conventional fluorophores, such as high signal-to-noise ratio and superior photostability. The up-converting materials are currently a subject of extensive research due to their prospective application in solar cells since a standard solar cell does not absorb in the NIR spectral range, as the energy of the NIR light is too low for injecting electrons into the conduction band of the solar cells semiconducting material. Another possible application is in optical imaging, as they allow excitation in the NIR spectral range where light absorption and scattering from biological tissues is minimized resulting in deep tissue penetration and low photodamage.

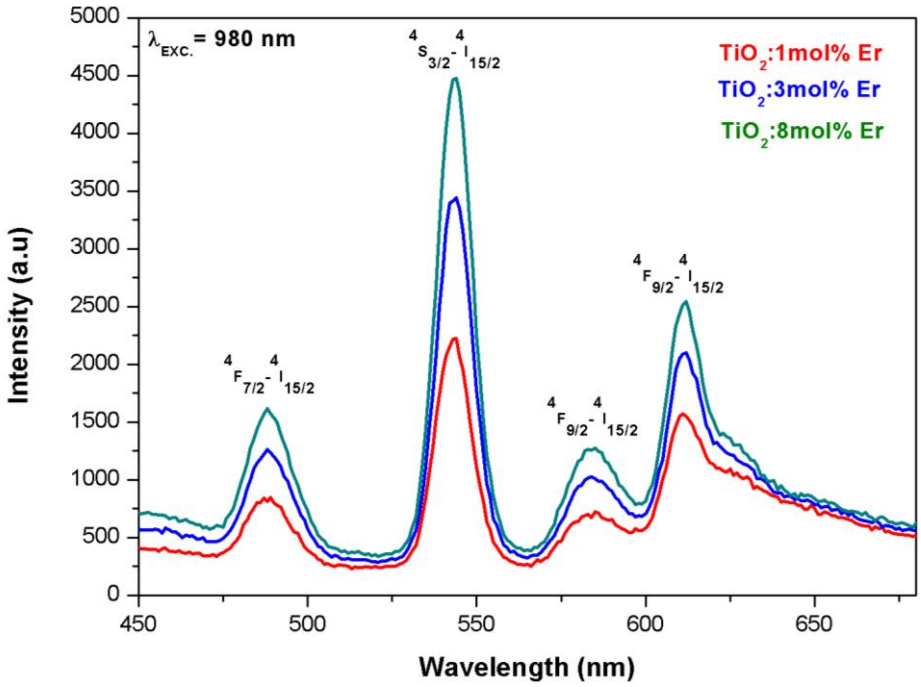

Figure 4.7: Up-conversion emission spectra for Er^{3+} doped TiO_2 nanoparticles under laser beam excitation of 980 nm.

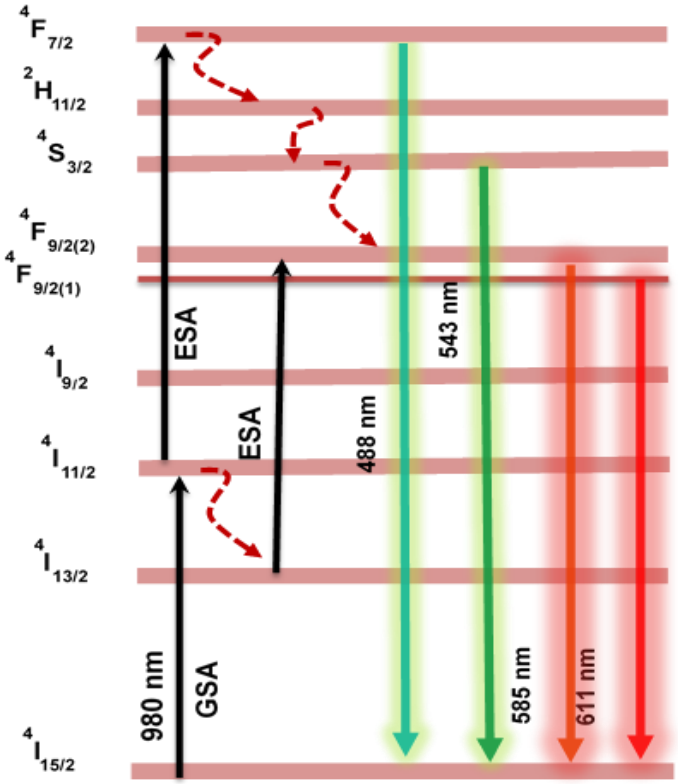

Figure 4.8: Energy level diagram for the up-converted luminescence from TiO_2 doped with Er^{3+} ions under infrared excitation at 980 nm.

4.4 Conclusion

Pure and Er^{3+} doped TiO_2 nanoparticles were successfully synthesized using the sol-gel method. The powder XRD spectra revealed that both synthesized pure and Er^{3+} doped TiO_2 nanoparticles remain in anatase phase after annealing at 400°C. From SEM and TEM observations, it was confirmed that the incorporation of Er^{3+} in TiO_2 decreases the grain size of the particles. UV-VIS/-NIR revealed a shift of band edge to higher wavelengths (red shift) with increasing Er^{3+} concentration indicating introduction of defects or impurity levels with Er^{3+} addition. Among Er^{3+} doped samples, the 1 mol% doped sample exhibited the highest down conversion PL emission intensity, while under NIR irradiation (980 nm), the optimal up-conversion luminescence intensity came from 8 mol% doping of Er^{3+} ions. This Er^{3+}doped TiO_2 nanoparticles have potential applications in various devices such as solar cells, light emitting devices, and bio imaging.

4.5 References

[1] Chen J, Zhao J.X., *Sensors* **2012**, *12*(3), 2414-2435.

[2] Salhi R, Deschanvres J-L., *J. Luminescence*, **2016**, 176, 250-259.

[3] Chatterjee D.K, Gnanasammandhan M.K., Zhang Y., *Small,* **2010**, 6(24), 2781-2795.

[4] Trupte T, Green M.A, Würfel P, *J. Appl. Phy.*,**2002**, 92(7), 4117-4122.

[5] de Wild J, Meijerink A, Rath J.K, van Stark W.G.J.H.M, Schropp R.E.I., *Energy Environ. Sci.,* **2011**, 4(12), 4835-4848.

[6] Singh V, Seshadri M, Singh N, Pathak M.S., Kumaran R.S, Choi Y.K., Singh P.K., Dhoble S.J., Srivastava A.K., *J. Lumin.* **2016,** 176, 347-355.

[7] Wang F, Lui X, *Chem. Soc. Rev.*, **2009**, 38(4), 976-989.

[8] Polman A, *J. Appl. Phys.* **1997**, 82(1), 1-39.

[9] Lallier E, *Appl. Opt.*, **1992**, 31(25), 5276-5282.

[10] Bahtat A, Bouazaoui M, Bahtat M, Garapon C, Jacquier B, Mugnier J, *J. Non-crystalline Solids.*, **1996**, 202, 16-22.

[11] Xu C.T, Zhan Q, Lui H, Somesfalean G, Qian J, He S, Andersson-Engels S. *Laser & Photonics Rev.*, **2013**, 7(5), 663-697.

[12] Thamaphat K, Limsuwan P, Ngotawornchai B, *Nat. Sci.,* **2008**, 42, 357-361.

[13] Reijnders L, *Polym. Degrad. Stabil.* **2009**, 94(5), 873-876.

[14] Fan K, Peng T.Y., Chen J, Zhang X.H., Li R.J., *J. Power Sources*, **2013**, 222, 38-44.

[15] Tojo S, Tachikawa T, Fujitsuka M, Majima T, *J. Phys. Chem.*, **2008**, 112(38), 14948-14954.

[16] Yang G, Jiang Z, Shi H, Xiao T, Yan Z, *J. Mater. Chem.*, **2010**, 20, 5301-5309.

[17] Irie H, Watanabe Y, Hashimoto K, *J. Phys. Chem. B.*, **2003**, 107(23), 5483-5486.

[18] Mor G.K, Shankar K, Paulose M, Varghesen O.K, Grimes C.A, *Nano. Lett.* **2006**, 6(2), 215-218.

[19] Patra A, Friend C.S, Kapoor R, Prasad P.N, *Chem. Mater*, **2003**, 15, 3650-3655.

[20] Polman A, van Veggel F.C.J.M, *J. Opt. Soc. Am. B.*, **2004**, 21(5), 871-892.

[21] Hufner S, *Optical spectra of transparent rare-earth compounds (Academic, New York, 1978)*

[22] Bunzli J-C, Chauvin A-S, *lanthanides in solar energy conversion, Handbook on the physics and chemistry of Rare Earths*, **2014**, 44, Elsevier B.V.

[23] Auzel F, *Chem. Rev.* **2004**, 104, 139.

[24] Zhang Q.F, Park J.T, Myers X.D, Cao, G.Z, *Adv. Energy Mater.* **2011**, 1, 988-1001

[25] Choy K.L, *Prog. Mater. Sci.*, **2003**, 48(2), 57-170.

[26] Ou H.H, Lo S.L, Liao C.H, *J. Phys. Chem.*, **2011**, 115(10), 4000-4007.

[27] Carp O, Huisman C.L, Reller A, *Prog. Solid State Chem.*, **2004**, 32(1), 33-177.

[28] Akpan U.G, Hameed B.H, *Applied Catalysis A: General*, **2010**, 375(1), 1-11.

[29] Tang Z.L, Zhang J.Y, Cheng Z, Zhang Z.T, *Mater. Chem. Phys.*, **2002**, 77(2), 314-317.

[30] Dai S, Wu Y, Sakai T, Du Z, Sakai H, Abe M, *Nanoscale Research Lett.* **2010**, 5, 1829-1835.

[31] Pal M, Pal U, Gonzalez R.S, Mora E.S, Santiago P, *J. Nano. Res.* **2009**, 5, 193-200.

[32] Lee D.K, Kim J.T, Park J-H, Kim Y-H, Lee I-K, Lee M-H, Kim B-Y, *Curr. Appl. Phys.* **2013**, 13, 1301-1305.

[33] Kabongo G.L, Mhlongo G.H, Mawela T, Mothudi B.M, Hillie K.T, Dhlamini M.S, *J. Alloys Compd.* **2014**, 591, 156-163.

[34] D.Y. Lee, M.-H. Lee, N.-I. Cho, *Curr. Appl. Phys.* **2012**, 12, 1229-1233.

[35] Sahu M, Biswas P, *Nano. Research Lett.* **2011**, 6(1), 441.

[36] Fitzgibbons E.T, Sladek K.J, Hartwig W.H, *J. Electrochem. Soc.* **1972**, 119, 735-739.

[37] Sole J.G, Bausa L.E, Jaque D, *An Introduction to the optical spectroscopy of inorganic solids.* **2005**, England: John Wiley and Sons Ltd.

[38] Kumar V, Ntwaeaborwa O.M, Holsa J, Swart H.C, *Opt. Mater.* **2015**, 46, 510-516.

[39] Ravaro L.P, Morais E.A, Scalvi L.V.A, Siu Li M, *Ceramica*,**2007**, 53, 187-191.

[40] Berggren K.F, Sernelius B.E, *Phys. Rev. B*, **1981**, 24(4), 1971-1986.

[41] Yang J , Hu Y, Jin C, Zhuge L, Wu X, *Thin Solid Films*, **2017**, 637, 9–13.

[42] Gultekin A, *Mater. Sci.* **2014**, 20(1), 10-14.

[43] Mercado C.C, Knorr F.J, Mchale J.L, Usmani S.M, Ichimura A.S, Saraf L.V, *J. Phys. Chem. C.* **2012**, 116, 10796-10804.

[44] Susmita P, Choudhury A, *Appl. Nanosci.* **2014**, 4(7), 839-847.

[45] Selman A.M, Hassan Z, *Superlattices Microstruct.* **2015**, 83, 549-654.

[46] Liu B, Zhao X, Wen L, *Mater. Sci. & Eng. B.* **2006**, 134, 27-31.

[47] Kabongo G.L, Mhlongo G.H, Mothudi B.M, Hillie K.T, Swart H.C, Dhlamini M.S, *Mater. Lett.* **2014**, 119, 71-74.

[48] Shi X.L, Wang S, Duan X.L, Zhang Q.X, *Mater. Chem. Phys.* **2008**, 112(3), 1110-1113.

[49] Nair P, Justinvictor V.B, Daniel G.P, Joy K, Raju K.C.J, Kumar D.D, Thomas P.V, *Progress in Natural Science: Materials International*, **2014**, 24, 218-225.

[50] Serpone N, Lawless D, Khairutdinov R, *J. Phys. Chem.* **1995**, 99(45), 16646-16654.

[51] Tshabalala Z.P, Motaung D.E, Mhlongo G.H, Ntwaeaborwa O.M, *Sensors and Actuators B*, **2016**, 224, 841–856.

[52] Choudhury B, Choudhury A, *Current App. Phys.* **2013**, 13, 1025-1031.

[53] Pal M, Pal U, Jimenez J.M.G.Y, Perez-Rodriquez F, *Nanoscale Res. Lett.* **2012**, 7(1), 1-12.

[54] Ding Y, Zhang X, Gao H, Xu S, Wei C, Zhao Y, *J. Alloys Compd.* **2014**, 599, 60-64.

Chapter 5: Sol-gel Synthesis and Characterization Studies of Er^{3+} Doped and Er^{3+}-Yb^{3+} Co-doped TiO_2 Nanoparticles

Erbium-doped and erbium-ytterbium co-doped titanium dioxide (TiO_2) nanoparticles were prepared via sol-gel synthesis method. The nanopowders were prepared with a fixed 8mol%Er concentration and various Yb concentrations. Result analysis of this chapter is mainly focused on comparison of pure TiO_2 and samples with most intense up-conversion luminescence (TiO_2: 8mol% Er^{3+} and TiO_2: 8mol% Er^{3+}-8mol% Yb^{3+}). The phase structure and particle size of TiO_2: Er^{3+} and TiO_2: Er^{3+}-Yb^{3+} nanocrystal samples were characterized by using x-ray diffraction (XRD) and transmission electron microscopy (TEM). The x-ray diffraction patterns confirmed the formation of an anatase TiO_2 phase. UV/Vis spectroscopy was used to measure the reflectance characteristics of the sample, and the band gap was extrapolated from Kubelka-Munk relation. Phonon quantification in TiO_2 was achieved using Fourier transform infrared (FT-IR) spectroscopy. The XPS technique was employed to confirm the formation of various defects. A laser beam with 980 nm wavelength was used to irradiate the sample, and the displayed emission lines of TiO_2: Er^{3+} in the visible region of the electromagnetic spectrum confirmed up-conversion luminescence. Enhancement of up-conversion luminescence intensity due to Yb^{3+} co-doping was observed, indicating an efficient Yb-Er energy transfer process.

5.1 Introduction

Development of new nanostructured up-converting materials with tailored physical and chemical properties is a promising technology for the remedy of environmental pollution and clean energy scarcity [1]. Up-converting materials based on rare-earth (RE) ions incorporated in appropriate host materials such as oxides, oxysulfides, and fluorides [2, 3] are gaining importance due to their capability to emit a detectable photon of higher energy from two or more low energy photons [4] for use in integrated optical devices (e.g., planar optical amplifiers [5] and low-cost near-infrared laser diodes [6, 7]. Materials with relatively low electron-hole recombination rate are considered as the most suitable hosts for RE ions for improving up-conversion luminescence because they can reduce multi-phonon non-radiative relaxation [3, 8]. To date, fluorides-based hosts have shown to enhance up-conversion luminescence intensity due to their high refractive index and high transparency arising from low-energy phonon however they suffer from auto-fluorescence and photodamage due to high excitation energy from the ultraviolet or visible light [9, 10].

These drawbacks have led to extensive studies towards oxide-based hosts due to their intriguing properties such as high chemical and high thermodynamic stability [11] under high current densities, high vacuum pressures and elevated temperatures [12]. Among oxide-based hosts, TiO_2 is the most commonly used rare earth doped semiconductor material for efficient near-infrared to visible up-conversion properties [3, 13]. TiO_2 has aroused extensive interest in recent years due to its many applications such as in solar cells [14], in gas sensors [15], and to purify air and water from contaminants [16]. In most of these applications, the particle size of TiO_2 plays a vital role in the performance of devices they are put in; consequently, much research has been focused on the reduction of the particle size towards the nanosized regime [17].

Naturally, TiO_2 exists in three main polymorphs of rutile (tetragonal), anatase (tetragonal), and brookite (orthorhombic) [18]. Rutile is usually stable at high temperatures (larger particle size), whereas anatase is stable at low temperatures (smaller particle size) leading to different physical properties which in turn, lead to different applications [19, 20]. Hence this study is focused on anatase phase due to its stability in the nano regime [18] and its relatively low phonon energy of 639 cm^{-1} [21].

There is an increasing demand for the properties of erbium as an up-converter due to its suitable electronic level scheme with nearly equidistant [22], long-lived excited states [3]. However, prior studies have shown that room temperature up-conversion emission from erbium in oxide-based hosts becomes diminished at high erbium concentrations [23]. On the other hand, due to less absorption; the up-conversion process has a low efficiency. However, much larger conversion efficiencies can be achieved by co-doping with another rare earth ion [24] and consequently in this study we investigate the up-conversion characteristics of TiO_2 nanoparticles doped with rare earth ion Yb^{3+}-Er^{3+} pair at different relative concentrations to yield the highest up-conversion luminescence emission output. Yb^{3+} has a very simple two-level energy system, consisting of one excited energy level $^2F_{5/2}$ around 980 nm [4] and it also possess a larger and spectrally broader absorption cross section than Er^{3+} [25]. To enhance the absorption of Er^{3+}, Yb^{3+} is used as a sensitizer, whereby Yb^{3+} absorbs and transfers energy to Er^{3+}, in which the emission occurs [26]. The $^2F_{5/2}$ level of Yb^{3+} has a long lifetime and it is also resonant with the $^4I_{11/2}$ of Er^{3+} [2].
In this study, Er and Yb co-doped titanium dioxide nanoparticles were successfully synthesized by the sol-gel method.

5.2 Experimental details

5.2.1 Sample preparation

Preparation of pure, Er^{3+} doped, and Er^{3+}-Yb^{3+} co-doped TiO_2 nanoparticles followed the same synthetic method as in **Chapter 4** (see **section 4.21**) and it is schematically presented in **Figure 5.1**.

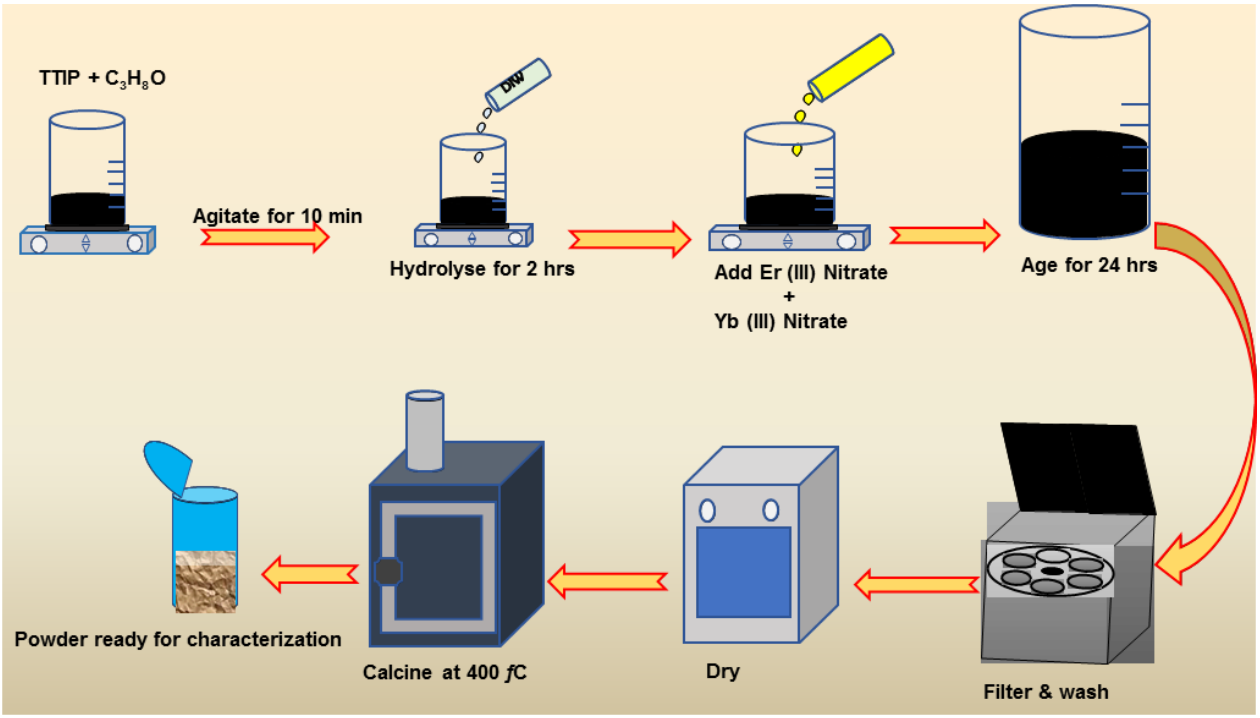

Figure 5.1: Schematic representation of the synthesis procedure of Er^{3+}-Yb^{3+} co-doped TiO_2 nanoparticles.

5.2.2 Characterization

The crystalline structure of nanopowders was examined at room temperature using CuKα (λ = 1.5406 Å) over the 2θ range from 10° to 90°. Phonon quantification in samples was achieved using Perkin Elmer FT-IR spectroscopy from 550 to 4000 cm^{-1}. The morphology and particle size of the samples were examined by transmission electron microscope (TEM). The XPS analysis was carried out with a Perkin-Elmer Phi 5600 ESCA to confirm various defects within the host lattice. The absorption characteristics of the powders were determined at room temperature using the 1050 UV-Vis-NIR spectrophotometer (Perkin Elmer) equipped with an integrating sphere. A continuous laser beam of 980 nm was used to excite the samples at room temperature using Fluorolog spectrometer (Jobin Yvon), and the emission was collected from 450 to 680 nm with a photomultiplier tube.

5.3 Results and Discussion

5.3.1 Structural and Surface properties

The XRD patterns for undoped, Er^{3+}, and Er^{3+}/Yb^{3+} co-doped TiO_2 nanocrystals, calcined at 400° C for 2 hours are shown in **Figure 5.2**.The XRD patterns are exclusively characteristic of anatase phase in agreement with JCPDS standard file #86-1157. Additionally, no peaks from erbium oxide or ytterbium oxide were observed. In general, the intensity of the diffraction peaks decreases greatly with the increase of doping content indicating a compromise of crystallinity due to lattice distortion (not shown). Peak broadening due to small crystallite size effect is observed with an increase in dopant content (follows same trend as XRD results presented in **Chapter 4**). However, from the Scherrer's formula (**Equation (5.1)**): for the (101) anatase peak, no significant change in crystallite sizes was found, this can be attributed to annealing but average crystallite size taken across all

diffracting modes indicate a systematic decrease in crystallite size with increasing dopant concentration.

$$D = k\lambda/\beta \cos\theta \qquad (5.1)$$

Where k = 0.9, D represents the crystallite size (Å), λ is the wavelength of Cu Kα radiation and β is the corrected half-width of the diffraction peak [4].

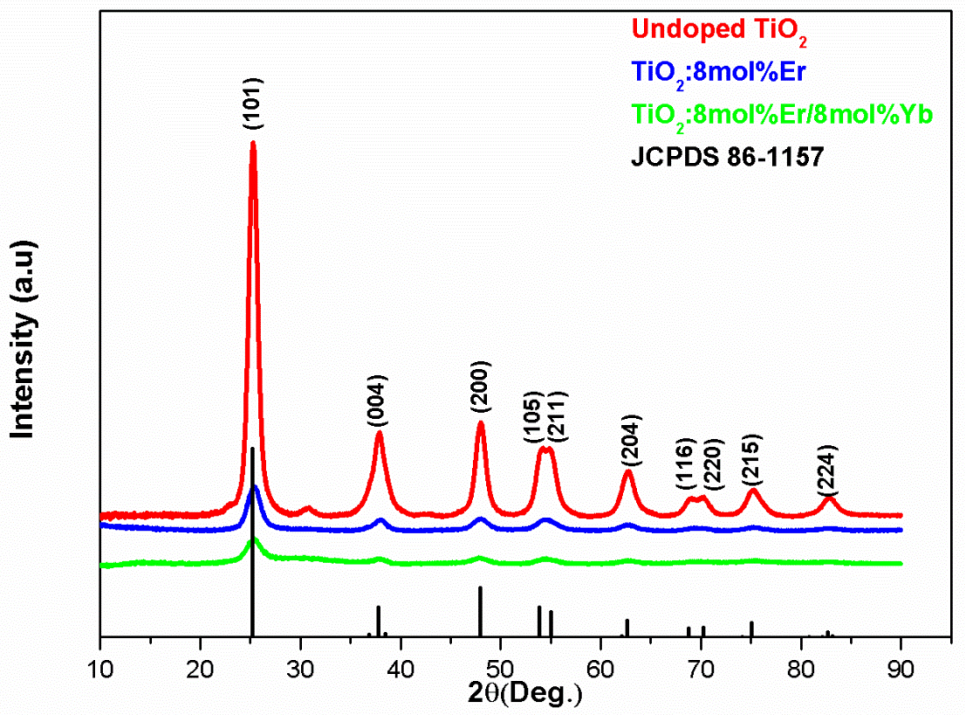

Figure 5.2: The XRD patterns of undoped, Er^{3+} doped and Er^{3+}/Yb^{3+} co-doped TiO_2 phosphor powders.

TEM analysis was employed to assess the size and morphology of the nanopowders. It is observed from TEM images that nanopowder samples consist of very small (quantum dot size) agglomerated nanoparticles which are spherical in shape (see **Figure 5.4**); this finding is in agreement with SEM image analysis (see **Figure 5.3**) and is consistent with the XRD result.

In recent years, spherical nanocrystalline aggregates have been reported to be improving the efficiency of solar energy conversion systems due to their ability to generate effective light scattering centers, comparable to the wavelengths of visible light [4, 28]. Additionally, it can be seen from the size distribution histograms that the average size of particles decreases with the increase of dopant content; this can be attributed to the formation of RE–O–Ti bonds in the doped samples, which inhibits the growth of crystal grains [29].

The decrease in particle size is more prominent in the co-doped samples since the dopants are at very high concentrations (8mol%Er-8mol%Yb), this concentration is chosen for its superior up-converting properties and this finding is also consistent with the peak broadening observed in the XRD result (see **Figure 5.2**).

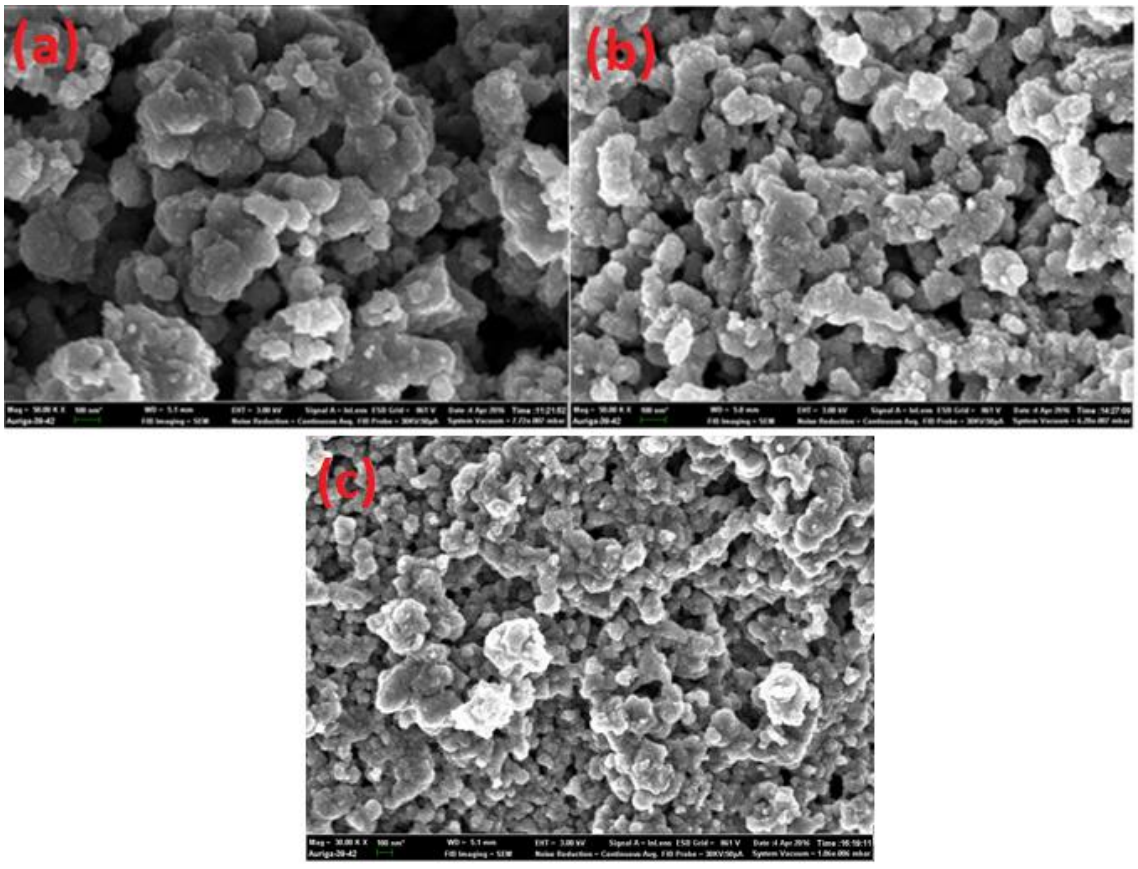

Figure 5.3: SEM micrographs of (a) undoped TiO_2, (b) 8mol% Er^{3+} doped and (c) 8mol% Er^{3+}-8mol%Yb^{3+} nanopowders**.**

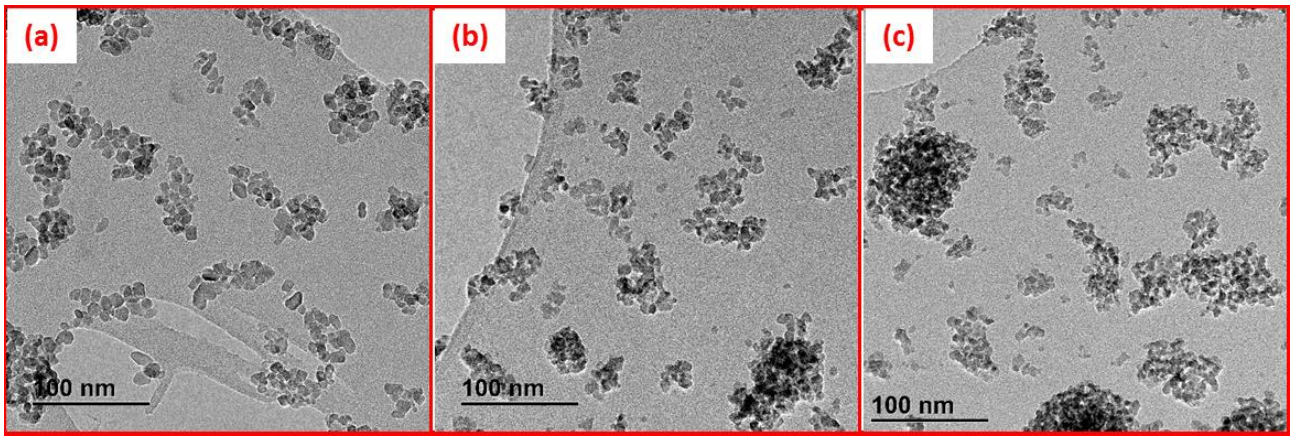

Figure 5.4: TEM images of **(a)** undoped, **(b)** 8mol% Er doped, and **(c)** 8mol%Er-8mol%Yb co-doped TiO_2**.**

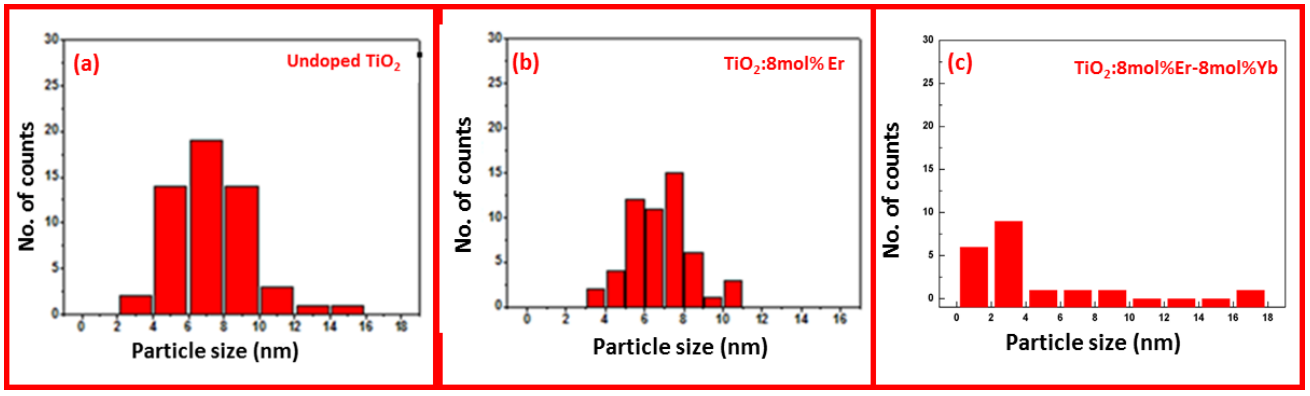

Figure 5.5: Particle size distribution of **(a)** undoped, **(b)** 8mol% Er doped and **(c)** 8mol%Er-8mol%Yb co-doped TiO_2 respectively.

XPS analysis was used to determine the main elements in the nanopowder samples. High-resolution XPS spectra of the Ti 2p core levels for undoped, Er^{3+}doped, and Er^{3+}/Yb^{3+} co-doped nanoparticles are shown in **Figure 5.6**. All the Ti 2p spectra show a doublet, whose binding energies are 464.6 and 458.8 eV; these peaks are attributed to Ti-$2p_{1/2}$ and Ti-$2p_{3/2}$, respectively. The distance between Ti-$2p_{1/2}$ and Ti-$2p_{3/2}$ is 5.8 eV, which indicates that titanium mainly existed as Ti^{4+} as shown in the table of literature values for Ti-2p spectra [30].

Table 5.1: Literature values for Ti-2p spectra.

Compound	Ti 2p3/2 (eV)	Std. Dev. (+/- eV)	# of Citations	Ti 2p1/2 - Ti 2p3/2 Splitting (eV)	Std. Dev. (+/- eV)	# of Citations
Ti(0)	453.9	0.3	8	6.1	0.06	2
Ti(II) Oxide	455.5	0.6	2	5.6		1
Ti(III) Oxide	457.3	0.7	2	5.2		1
Ti(IV) Oxide	458.7	0.2	13	5.7	0.08	4

It can also be seen that there is a slight shift to lower binding energies for the doped samples as compared to undoped TiO_2 sample, this shift can be ascribed to the change of local chemical environment of Ti ions due to the incorporation and the formation of RE–O–Ti bonds on the surface of TiO_2 [31].

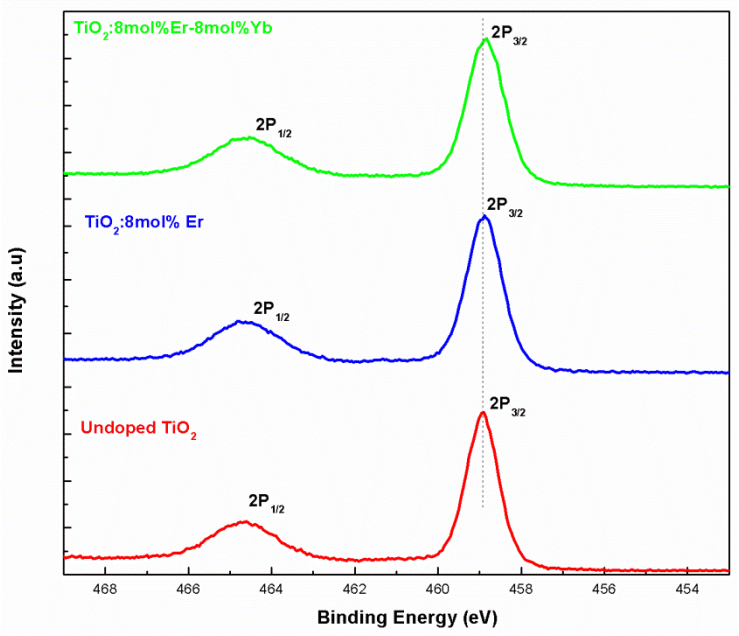

Figure 5.6: High-resolution XPS spectra of the Ti 2p core levels for undoped, Er^{3+} doped, and Er^{3+}-Yb^{3+} co-doped TiO_2 nanocrystals.

The deconvoluted oxygen O1s peaks for 0, 8mol%Er and 8mol%Er-8mol%Yb doping of TiO_2 nanopowders are shown in **Figure 5.7**, indicating the existence of more than one chemical state convoluted in these spectra (O1, O2, and O3). The peak O1 is characteristic of lattice oxygen (Ti–O bond) i.e. an oxygen atom bound to the Ti^{4+} ions array [31, 32]. The peak O2 is associated with O^{2-} ions that are in oxygen deficient regions in the matrix of TiO_2 [32].

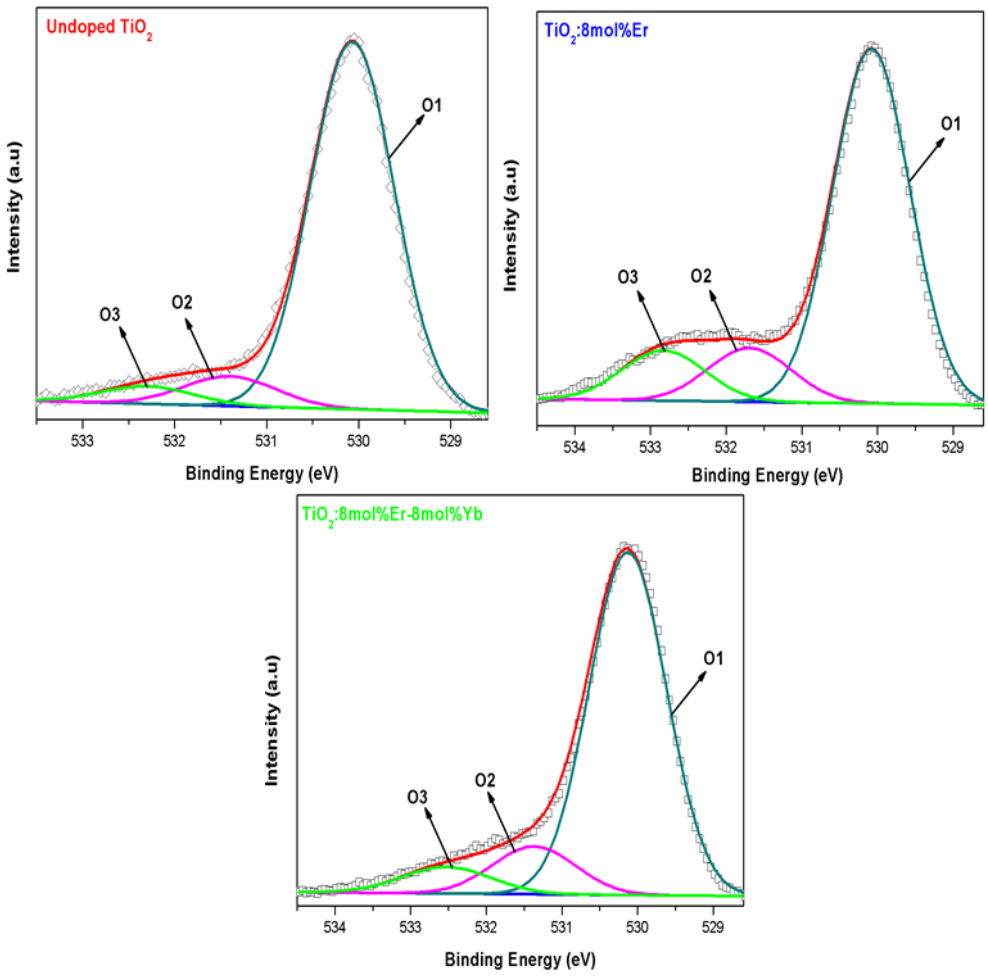

Figure 5.7: Deconvolution of the O1s peak of undoped, 8mol%Er doped and 8mol%Er-8mol%Yb co-doped TiO_2 nanocrystals.

Table 5.2 shows the effect of doping and co-doping on the peak position and area of the O1s peak.

Table 5.2: Peak positions and areas for different O1s peaks.

Sample (mol. %)	Peak Name	Peak Position (eV)	Area (%)
0	O1	530.07	87.4
	O2	531.4	7.9
	O3	532.4	4.7
8(Er)	O1	530.08	75.9
	O2	531.6	12.5
	O3	532.5	11.6
8(Er)-8(Yb)	O1	530.1	80.6
	O2	531.4	12.2
	O3	532.5	7.2

Figure 5.8 shows the FT-IR spectra of the prepared undoped, Er^{3+} doped, and Er^{3+}/Yb^{3+} co-doped TiO_2 nanopowders. The spectra comprised of three main absorption bands in the region of 650-850 cm^{-1}, 1500-1700 cm^{-1}, and 2680-3750 cm^{-1}. The bands in the low energy region are assigned to the Ti–O–Ti vibrations corresponding to the presence of TiO_6 group [33].

The bands in the range of 3200 cm^{-1} are characteristic of the OH^- vibrations of physically absorbed molecular water and the bands between 1500-1700 cm^{-1} are attributed to υ[C=C, C=O] and δCH_3 vibrations, which correspond to the organic residues [33]. It is also observed that the peaks of undoped TiO_2 are much stronger than those of doped samples.

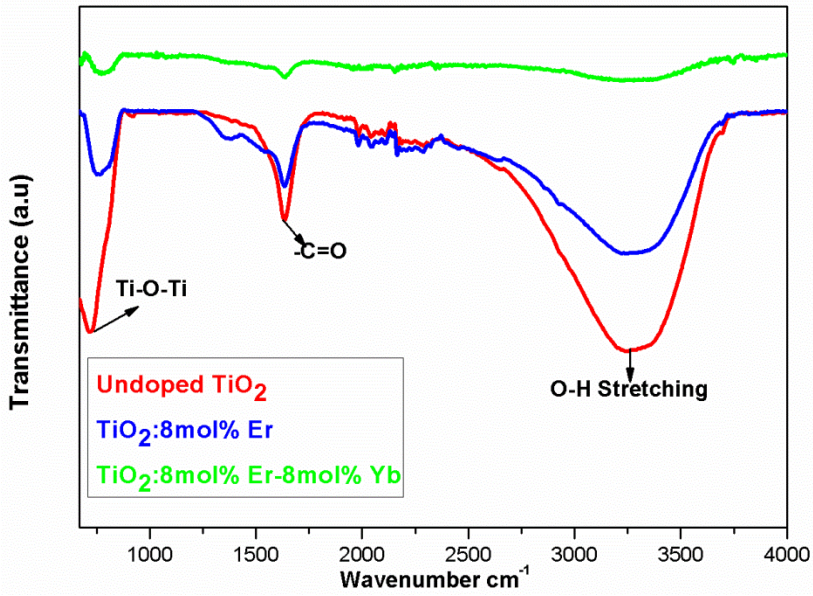

Figure 5.8: FT-IR transmittance spectra of undoped, Er^{3+} doped, and Er^{3+}/Yb^{3+} co-doped TiO_2 nanopowders**.**

5.3.2 Optical Characterization

To study the optical absorption properties of nanopowder samples, diffuse reflectance absorption spectra (DRS) in the range of 200-1000 nm were investigated. **Figure 5.9** show that undoped TiO_2 has no absorption band which is characteristic of visible light absorption. However, it has a sharp absorption band edge in the region of 350 nm-this band edge can be ascribed to the intrinsic relatively large band absorption of TiO_2 consistent with UV light absorption [32].

The absorption band edge of undoped TiO_2 does not shift significantly after incorporation of erbium and ytterbium at higher concentrations in contrast to lower concentrations. However, there are five distinct peaks observed in the absorption spectra of doped samples at ≈ 453, 490, 523, 544, and 654 nm corresponding to transitions of Er^{3+} from ground state $^4I_{5/2}$ to the excited states indicated in **Figure 5.9**.

Additionally, there is one peak at around ≈ 980 nm which is characteristic of absorption of light in the NIR region, this peak is enhanced after co-doping with Yb, indicating energy transfer between the sensitizer Yb to the activator Er ions. The absorbance of Er^{3+} around 980 nm can be increased by co-doping with Yb^{3+} since the absorption cross section of Yb^{3+} at 980 nm is larger than that of Er^{3+}, and its absorption band extends over a wider wavelength region, between 850 nm and 1000 nm as seen in **Figure 5.9**.

The optical band gap of TiO_2 was estimated using Kubelka-Munk relation by plotting $[F(R)*h\upsilon]^2$ vs $h\upsilon$ (see **Figure 5.10**). The results indicate that the band gap energy of undoped TiO_2 is 3.47 eV, 3.44 eV and 3.48 eV with the doping of erbium (red shift) and the co-doping of ytterbium (blue shift), respectively. It has already been observed (see **Chapter 4)** that in general the band gap is narrowed by incorporation of Er into TiO_2 host lattice, thus the band gap narrowing from undoped TiO_2 to 8 mol% Er content as observed (see **insert of Figure 5.10**). The band gap widening of 8 mol%Er-8 mol% Yb into TiO_2 lattice may be either attributed to (i) particle size reduction, (ii) variation in carrier concentrations and carrier scattering by micro-structural defects, grain boundaries, and ionic impurities, and (iii) lattice distortion due to incorporation of larger Er^{3+}-Yb^{3+} ions in TiO_2 lattice.

The widening of the band gap, in this case, can be associated with the 'Burstein-Moss effect', the effect in which the Fermi level of heavily doped n-type semiconductors can be located in conduction band E_c + dE, in this case; the optical transitions of electrons from valence band can take place only to the energy levels in conduction band located above the Fermi level since energy levels below the Fermi level are filled with electrons. Therefore, the location of the self-absorption edge shifts towards higher energy and thus the effective band gap is equal to E_g + dE (i.e. it increases) [34].

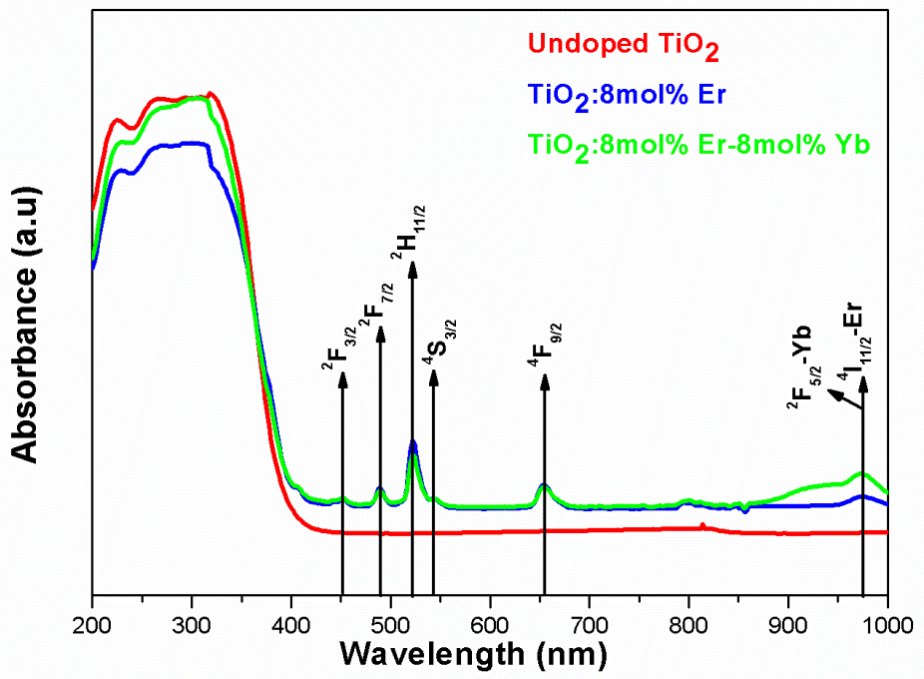

Figure 5.9: UV/Vis/NIR absorption spectra of nanopowder samples.

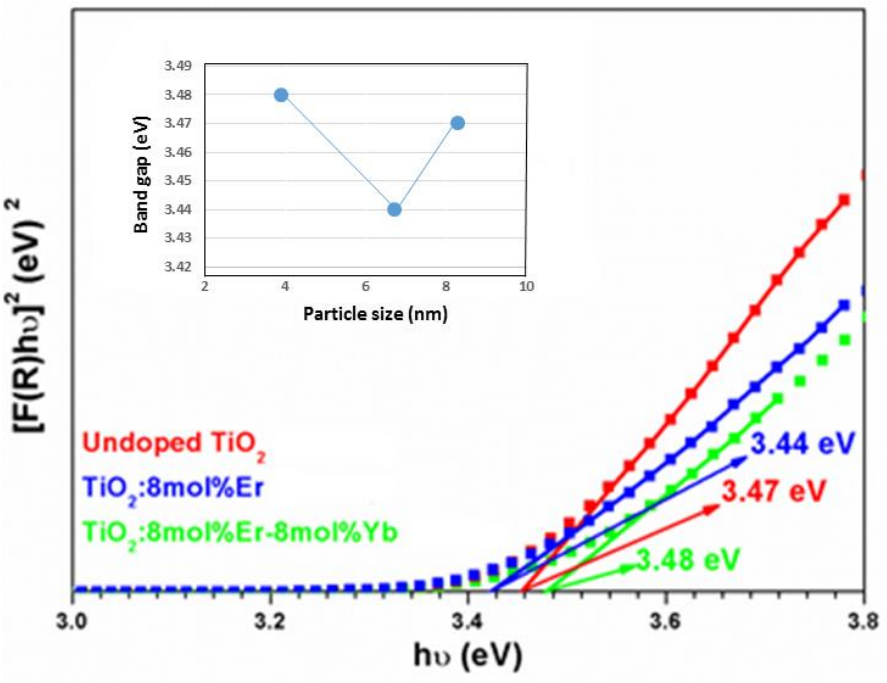

Figure 5.10: The band gap estimation using Kubelka-Munk relation for nanopowder samples. The insert shows the dependence of the band gap on the particle size.

Figure 5.11 shows photoluminescence PL emission spectra of the prepared undoped, Er^{3+} doped, and Er^{3+}-Yb^{3+} co-doped TiO_2 samples at various concentrations under excitation wavelength of 320 nm. Similarly to Er^{3+} singly doped TiO_2, two bands peaked at 374-378 nm and 435-438 nm are observed, corresponding to band-to-band recombination and defect related emissions, respectively [35]. It is observed that singly doped TiO_2 has the sharpest and most intense UV emission peaks (see **Chapter 4**) simply because in doubly doped materials, the separation between the impurity ions is reduced leading to transfer of energy among them and not with the host lattice and consequently resulting in a non-radiative process, hence the luminescence is quenched [36].

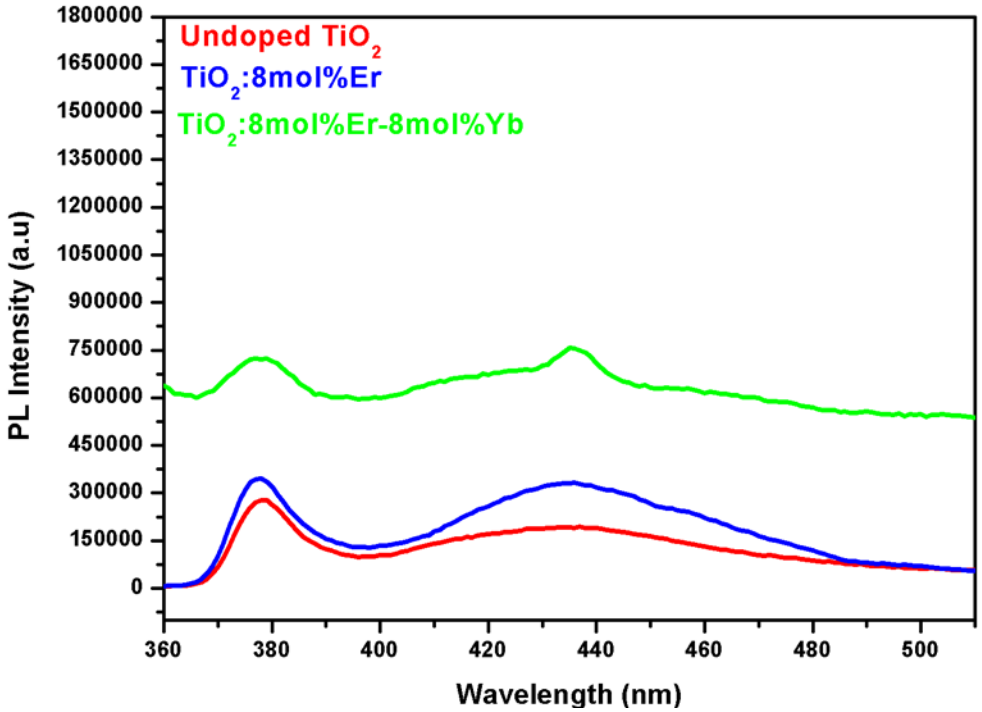

Figure 5.11: PL emission spectra of prepared nanopowder samples.

Up-conversion photoluminescence emission spectra of TiO_2 doped at various concentrations with excitation under 980 nm at room temperature is shown in **Figure 5.12**. No up-conversion luminescence was detected for undoped TiO_2 (not shown), this is attributed to a relatively large band gap of TiO_2 making it insensitive to NIR light. The Er doped TiO_2 emission spectrum consists of intense green light emission (central wavelength of 543 nm) corresponding to Er^{3+}: $^4S_{3/2} \rightarrow {}^4I_{15/2}$ transition [3]. There are other additional three emissions peaks observed at 488 nm, 585 nm, and 611 nm; these can be attributed to $^4F_{7/2} \rightarrow {}^4I_{15/2}$, $^4F_{9/2} \rightarrow {}^4I_{15/2}$ and $^4F_{9/2} \rightarrow {}^4I_{15/2}$ Er^{3+} transitions, respectively. It is also noted that the strongest up-conversion emission intensity is attributed to the nanopowder co-doped with 8mol%Yb, indicating an effective Yb-Er energy transfer process (luminescence intensity quenches at concentrations above 8mol% Yb as shown in **Figure 5.12**). These emissions take place due to the optically active center of Er/Yb in the TiO_2 lattice with a local structure similar to that of the ErO_6 unit [37].

Yb^{3+} has only two energy levels, which can effectively suppress undesired non-radiative recombination where the energy loss of the absorbed incident light may happen. It has been reported that the photon energy in NIR region can be efficiently transported from the sensitizer Yb to the activator Er, thus promoting electrons of Er to the high-lying energy, followed by up-conversion emission of high photon energy through radiative transitions [37]. In most cases, the up-conversion emission process of Er^{3+} can be explained by two basic predominant mechanisms: excited state absorption (ESA) and energy transfer up-conversion (ETU) [23].

The energy transfer mechanism from Yb to Er resulting in enhanced up-conversion luminescence in the green region (525-560 nm) can be explained as follows: Yb^{3+} at $^2F_{7/2}$ ground state absorbs light and it is excited to $^2F_{5/2}$ energy level by ground state absorption (GSA), when Yb^{3+} at the excited state recombines non-radiatively to the ground state, its energy is transferred to neighboring Er^{3+} ion in the $^4I_{11/2}$ state which is resonant with $^2F_{5/2}$ level of Yb^{3+}, and then this already excited Er^{3+} ions to the $^4F_{5/2}$ ($^4H_{11/2}$) through the following channel: $^4I_{11/2} \rightarrow {}^4F_{5/2}$. This is the main pathway by which Yb^{3+} sensitizes the up-conversion process by energy transfer. The transition from $^4S_{3/2}$ excited state to the ground state results in the green emission in the region of 525-560 nm as seen in **Figure 5.12**. There are other possible pathways of up-conversion emission that can take place since the excited state Er^{3+} at the ground $^4I_{15/2}$ state may be populated after different excitation energy transition and relaxation because of the large Er^{3+} and Yb^{3+} concentration in our samples. The possible mechanism of energy transfer occurring in Er^{3+}/Yb^{3+} co-doped TiO_2 nanophosphors is shown in **Figure 5.13**.

Materials produced from this study have potential applications in optical devices, such as color display, optical data storage, photovoltaic solar cells and biomedical diagnostics.

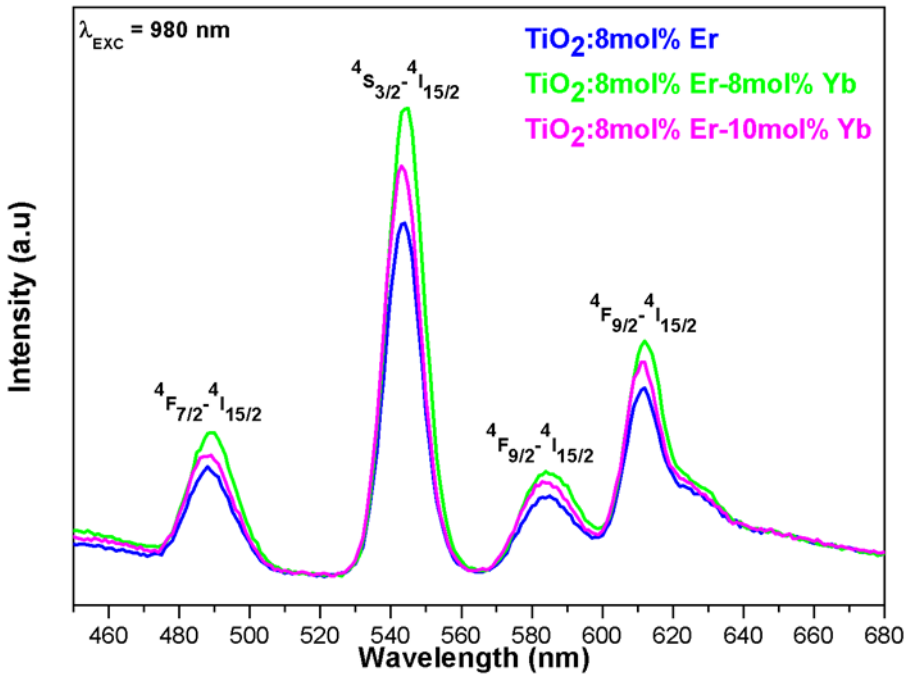

Figure 5.12: Up-conversion emission spectra for Er^{3+} doped and Er^{3+}/Yb^{3+} co-doped TiO_2 nanopowders in the wavelength range 500-680 nm under laser beam excitation of 980 nm.

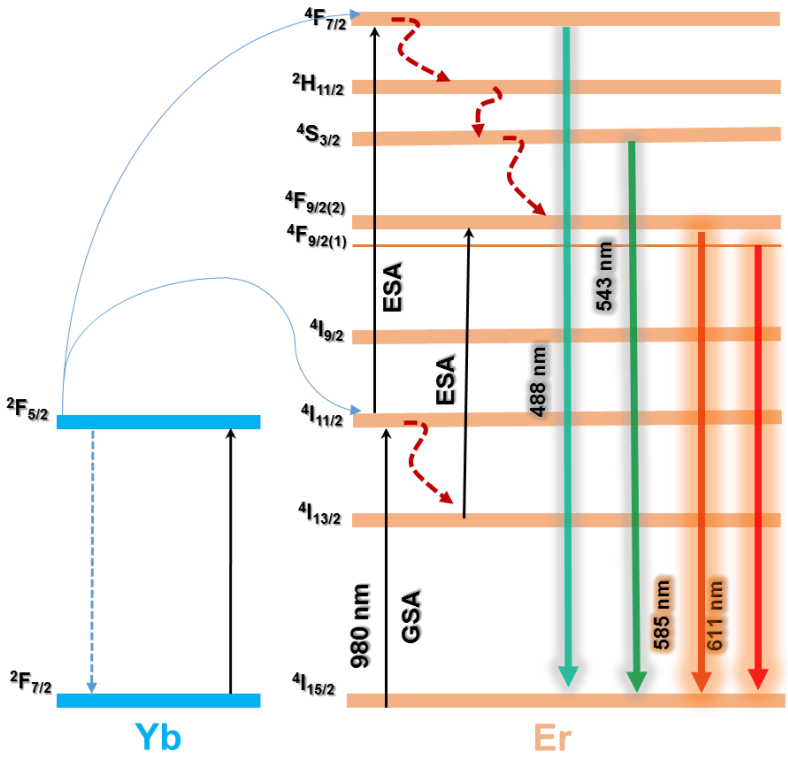

Figure 5. 13: The possible energy transfer mechanism occurring in Er^{3+}-Yb^{3+} co-doped TiO_2 nanophosphors.

5.4 Conclusion

Er^{3+} doped and Er^{3+}-Yb^{3+} co-doped TiO_2 nanopowders were successfully synthesized by sol-gel method. The powder XRD spectra revealed that all undoped and doped nanopowders remain in anatase phase after annealing at 400° C. The formation of different kinds of defects was confirmed by XPS measurements. The optimized TiO_2:8mol%Er-8mol%Yb nanopowder was found to possess the strongest up-conversion than other nanopowders. Enhancement of up-conversion luminescence intensity due to Yb co-doping was observed, indicating an efficient Yb-Er energy transfer process. The up-conversion luminescence intensity decreases with the increase in dopant concentration inferring there is an optimum concentration of the dopant to show strong emission peaks. Nanoparticles produced from this study are promising candidates for strong green emission.

5.5 References

[1] Pal M, Pal U, Gonzalez R.S, Mora E.S, Santiago P, *J. Nano Research,* **2009**, 5, 193-200.

[2] de Wild J, Meijerink A, Rath J.K, van Stark W.G.J.H.M, Schropp R.E.I., ***Energy Environ. Sci.,*** **2011**, 4(12), 4835-4848.

[3] Singh V, Seshadri M, Singh N, Pathak M.S., Kumaran R.S, Choi Y.K., Singh P.K., Dhoble S.J., Srivastava A.K., *J. Lumin.* **2016,** 176, 347-355.

[4] Salhi R, Deschanvres J-L., *J. Lumin.,* **2016**, 176, 250-259.

[5] Kitagawa T, Hattori K, Shimizu M, Ohmori Y, Kobayashi M, *Electron. Lett.***1991**, 27, 334.

[6] Nykolak G, Haner M, Becker P.C, Shmulovich J, Wong Y.H, *IEEE Photonics Technol. Lett.* **1993**, 5, 1014.

[7] Feuchter T, Mwarania E.K, Wang J, Reekie L, Wilkinson J.S, *IEEE Photonics Technol. Lett.* **1992**, 4, 1818.

[8] Xiao Q, Si Z, Zhang J, Xiao C, Yu Z, Qiu G, *J. Mater. Sci.* **2007**, 42, 9194.

[9] Chen J, Zhao J.X., *Sensors* **2012**, *12*(3), 2414-2435.

[10] Yang J, Deng Y, Wu Q, Zhou J, Bao H, Li Q, Zhang F, Li F, Tu B, Zhao D, *Langmuir,* **2010**, 26, 8850-8856.

[11] Ren G, Lan J, Zeng C, Liu Y, Zhan B, Butt S, Lin Y-H, Nan C-W, *JOM,* **2015**, 67, 211-221.

[12] Tay B.K, Zhao Z.W, Chua D.H.C, *Mater. Sci. & Eng. R.* **2006**, 52, 1-48.

[13] Huang S, Lou Z, Qi Z, Zhu N, Yuan H, *App. Catal. B-Environ.* **2015**, 168-169, 313-321.

[14] Lee K.M, Hu C.W, Chen H.W, Ho K.C, *Sol. Energ. Mat. Sol. C.* **2008**, 92, 1628-1633.

[15] Gyorgy E, Socol G, Axente E, Mihailescu I.N, Ducu C, Ciuca S, *Appl. Surf. Sci.* **2005**, 247, 429-433.

[16] Ao C.H, Lee S.C, *Chem. Eng. Sci.* **2005**, 60, 103-109.

[17] Thamaphat K, Limsuwan P, Ngotawornchai B, *Nat. Sci.,* **2008**, 42, 357-361.

[18] Li W, Ni C, Lin H, Huang C.P, Shah S.I, *J. Appl. Phys.* **2004**, 96(11), 6663-6668.

[19] Gribb A.A, Banfield J.F, *Am. Mineral.* **1997**, 82, 717-728.

[20] Zhang H.Z, Banfield J.F, *J. Mater. Chem.* **1998**, 8, 2073-2076.

[21] Bahtat A, Bouazaoui M, Bahtat M, Garapon C, Jacquier B, Mugnier J, *J. Non-crystalline Solids.*, **1996**, 202, 16-22.

[22] Hufner S, *Optical spectra of transparent rare-earth compounds (Academic, New York, 1978).*

[23] Abedrabbo S, Mohammed Q, Fiory A.T, *Appl. Surf. Sci.,* **2009**, 225(8), 4503-4511.

[24] van Stark W.G.H.M, Meijerink A, Schropp R.E.I, Solar spectrum conversion for photovoltaics using nanoparticles in third generation photovoltaics, Fthenakis‘ V, Editor., **2012**, In Tech.

[25] Strohhofer C, Polman A, *Opt. Mater.* **2003**, 21, 705-712.

[26] Krämer K, Biner D, Frei G, Gudel H, Hehlen M, S. Luthi, *Chem. Mater.* **2004**, 16, 1244-1251.

[27] Jeon S, Braun P.V, *Chem. Mater.* **2003**, 15, 1256-1263.

[28] Salhi R, Roussel H, Chaudouet P, Maalej R, Fourati M, Deschanvres J-L, *Chem. Vap. Depos.* **2011**, 17, 93.

[29] Xu A-W, Gao Y, Liu H-Q, *J. Catal.,* **2002**, 207, 151-157.

[30] Crist B.V, *XPS Reports*, **2007**, 1, 1-52.

[31] Fengping H, Shuai W, Shuang Z, Yingee F, Chunxue L, Chuang W, Chun L, *Bull. Korean Chem. Soc.* **2014**, 35(8), 2512-2518.

[32] Kumar V, Ntwaeaborwa O.M, Holsa J, Motaung D.E, Swart H.C, *Opt. Mater.* **2015**, 46, 510-516.

[33] Fitzgibbons E.T, Sladek K.J, Hartwig W.H, *J. Electrochem. Soc.* **1972**, 119, 735-739.

[34] Kabongo G.L, Mhlongo G.H, Mawela T, Mothudi B.M, Hillie K.T, Dhlamini M.S, *J. Alloys Compd.* **2014**, 591, 156-163.

[35] Ruso J.M, Verdinelli V, Hassan N, Messina P.V, *Langmuir.*, **2013**, 29, 2350-2358.

[36] Sole J.G, Bausa L.E, Jaque D, *An Introduction to the optical spectroscopy of inorganic solids.* **2005**, England: John Wiley and Sons Ltd.

[37] Sun J, Zhang W, Zhang W, Du H, *Mater. Res. Bull.* **2012**, 47, 786.

Chapter 6: Conclusion and Future Works

6.1 Conclusion

This study describes an easily controlled Sol-Gel route of synthesizing nanocrystalline TiO_2 powder. Calcined powders are characterized for their phases, structural and optical, elemental and morphological properties using different characterization techniques such as XRD, TEM, SEM-EDX, XPS, FT-IR, UV/Vis/NIR and PL spectroscopy.

This chapter is divided into two studies: the first is dedicated to the studies based on optimization of erbium doped TiO_2 nanopowders and the second focuses on the enhancement of optical properties of TiO_2: Er^{3+} nanoparticles by co-doping with a sensitizer Yb^{3+}. Findings from this research are outlined below:

Nanocrystalline luminescent TiO_2: RE^{3+} powders can be successfully synthesized through a simple Sol-Gel process of hydrolyzing titanium tetra-isopropoxide (TTIP) in a mixture of isopropanol and deionized water. 400° C was selected as an optimum calcination temperature to exclusively obtain TiO_2 anatase phase structure. Crystallite size was first estimated through XRD, then confirmed by HR-TEM and found to be in the quantum dots range.

The EDX and XPS elemental analysis were used to investigate the chemical composition of the prepared samples. Phonon quantification in TiO_2 samples was achieved using the FT-IR spectroscopy. UV/Vis/NIR spectroscopy was employed to study optical properties of the samples; the shift in the absorption band edge due to doping was observed indicating the tunability of the band gap of the prepared TiO_2 nanopowders, the band gap was estimated by Kubelka-Munk relation.

Furthermore, photoluminescence study on the prepared samples evidenced the presence of energy transfer between the rare earth dopant and the TiO_2 host matrix, the efficiency of this energy transfer is highly dependent on the concentration of the dopant i.e. there exists an optimum dopant content level at which strongest emission peaks are observed. Finally, the dependence of up-conversion luminescence intensity from Er^{3+} on the TiO_2 host structure was studied by using photoluminescence spectroscopy equipped with a continuous laser beam with 980 nm wavelength. The up-conversion luminescence intensity from TiO_2: Er^{3+} nanocrystals was enhanced by co-doping with the sensitizer Yb^{3+} due to the larger absorption cross section of Yb^{3+} compared to Er^{3+}.

6.2 Future Works

The current area of interest in this study has been the modification of TiO_2 nanocrystals sensitivity to visible light and beyond (NIR) while also studying their structural and elemental properties. In this study, TiO_2 was doped with erbium and ytterbium, in future this can be extended to other rare earth ions such as holmium and thulium, etc. moreover development of a synthesis method to incorporate these dopants should be done thoroughly since the impurity sites in the host matrix are mainly created during preparation, in line with this; a method of fabrication TiO_2 nanocrystals that can control size, shape, and spacing of the nanoparticles in a reproducible manner on a large scale must be identified. In particular microwave assisted method is an ideal candidate going forward. Finally, after the optimization of these materials, a study will be conducted to examine the feasibility of applying these nanoparticles in various fields of nanotechnology such as solar cells, light emitting devices, and application in bio-medical fields.

6.3 Conferences

- T. Talane, P.S Mbule, L.L Noto, G.H Mhlongo, B.M Mothudi, M.S Dhlamini, Up-conversion emissions of Er^{3+} doped and Er^{3+}/Yb^{3+} co-doped TiO_2 nanoparticles prepared by sol-gel method, SOS Symposium, September 2016, UNISA.

- T. Talane, P.S Mbule, L.L Noto, G.H Mhlongo, B.M Mothudi, M.S Dhlamini, Sol-gel Synthesis and Characterization Studies of Er^{3+} doped TiO_2 nanoparticles, 61st Annual Conference of the South African Institute of Physics (SAIP), 4-8 July 2016, University of Cape Town.

- T. Talane, P.S Mbule, L.L Noto, G.H Mhlongo, B.M Mothudi, M.S Dhlamini, Sol-gel Synthesis and Characterization Studies of Er^{3+} doped TiO_2 nanoparticles, DST-NRF Nanotechnology Symposium, 27 June 2016, CSIR.